

1

A brief introduction to strongly correlated electronic materials

E. DAGOTTO AND Y. TOKURA

1.1 Motivation

A brief introduction is presented to the very active field of research that addresses the properties of strongly correlated electronic materials. Our focus is on the complex transition-metal oxides, with emphasis on the manganese oxides known as manganites, but also describing several other materials, such as high-temperature superconductors and multiferroic compounds. In these correlated electron materials the interactions between the electronic spins, their charges and orbitals, and the lattice produce a rich variety of electronic phases and self-organization. The competition and/or cooperation among these correlated electron phases can lead to the emergence of surprising electronic phenomena and also of interesting functionalities via their nonlinear responses to external fields, potentially forming the basis for a new type of electronics. Our perspective on future interesting directions in this area of research is also included in this chapter.

1.2 Introduction

The study of Strongly Correlated Electronic (SCE) materials is among the most exciting, and challenging areas of research in condensed matter physics [1, 2]. In these materials the behavior of their conduction electrons cannot be described merely by using non-interacting components, as in the often employed one-electron approximation to good metals such as silver or copper. Other sophisticated approaches, including the local-density approximation to density functional theory, are still one-electron theories, and in general they are not applicable to the proper understanding of SCE compounds, particularly at low temperatures. In this family of materials an electron cannot simply be considered to be immersed in the average “mean field” of the others. A typical example is provided by NiO which has a partially filled $3d$ band and, for this reason, it should be a metal. However, the Coulomb repulsion between electrons, that induces nontrivial correlations among them, renders NiO an insulator [3].

4 A brief introduction to strongly correlated electronic materials

In the absence of one-particle approximations, theoretical studies of SCE materials are usually carried out using model Hamiltonians, where the dominant terms often correspond to the electrons interacting with one another via Coulomb interactions (that are often assumed to be local in real space, namely on a lattice site or involving nearest neighbor sites, after consideration of screening effects). Coupling with lattice vibrations can also be very important if it is strong. In these model Hamiltonians the electronic movement involving tunneling of electrons between atoms is incorporated via the so-called tight-binding hopping terms.

The complete models including all of these terms are still deceptively simple to write, but solving them, even approximately, requires an enormous effort since many-body SCE systems typically do not have a small parameter to expand on. For this reason, the use of computational techniques is gradually acquiring increasing importance for the theoretical study of this type of material, as discussed in more detail later in this chapter. The above mentioned difficulty in reaching a theoretical understanding of SCE materials, and even of idealized SCE model Hamiltonians, also arises from the several different physical states that are in close competition in these compounds, often involving metals and insulators that can be so close in energy that small external electric or magnetic fields may induce nonlinear responses caused by transitions from one to the other. So a proper theoretical description not only needs good handling of the ground state under investigation, but also of excited states that may have quite different properties [1, 2].

It is clear that SCE materials represent a challenging and exciting frontier for solid state physics: while the understanding of their properties is difficult, their potential applications could be very interesting. These materials can be found in complex states such as high temperature superconductors and heavy fermions, and they can be very susceptible to small perturbations such as in the case of colossal magnetoresistance found in manganese oxides, where relatively small magnetic fields of a few Teslas, which are small in typical electronic energy scales, induce huge changes of many orders of magnitude in resistivity.

The current chapter provides a brief overview of this vast area of research, known colloquially as “strongly correlated electrons”. It is important that the reader should be aware that in a single chapter it would be impossible to address all of the many exciting topics of research contained within this field. As a consequence, the authors have focused on the subset with which they have developed their own scientific area of expertise, and for this reason they will mainly address transition-metal oxides. This focus, with an emphasis on bulk materials, will nevertheless be useful to better understand some of the other chapters in this book that also specialize in transition-metal oxides, although in the form of artificially engineered superlattices. It is also important to remark that topics that are still controversial, such as the actual origin of high temperature superconductivity in cuprates, will be only briefly reviewed here, with sufficient references to allow the reader to arrive at their own conclusions on this subfield. Thus, emphasis will be given to particular areas of research, such as colossal magnetoresistance, where in recent years considerable progress has been made and consensus reached due to a remarkable cross fertilization between theoretical and experimental efforts. The chapter ends with our opinion about the present status of the SCE field of research and its future.

The current chapter is based on a recent review article by the authors [4], but it incorporates considerable additional information and several references not included in that previous publication. As expressed before, ours is certainly not a comprehensive review and, moreover,

for simplicity the cited literature is naturally biased towards the publications by the authors. As a consequence, readers that are interested in developing a more profound understanding of SCE materials, beyond the information contained in this chapter, are urged to consult the additional literature that is cited in the list of publications at the end of this chapter.

1.3 Why correlated electrons?

As mentioned in the introduction, one of the most intensively studied areas of research in condensed matter physics is the field of SCE materials [1, 2, 4]. Why are these compounds considered to be such an interesting challenge? Typically, SCE materials are made of simple building blocks, such as transition-metal ions located inside an octahedral oxygen cage forming, by periodic repetition, an overall lattice perovskite structure. However, the large ensemble of these constituents behaves in a nontrivial complex manner, leading to collective responses that are quite difficult to predict *a priori* based on the properties of those small octahedral building blocks. Typical examples are the high temperature superconductivity that exists in layered copper oxides and the colossal magnetoresistance of manganites, to be described in more detail later in this chapter. As mentioned before, in these SCE systems the collective states cannot be understood based on the one-electron (or even one-quasiparticle) approximation, even if the calculations are fully quantum mechanical. The mere addition of the individual electronic properties is not sufficient to rationalize the subtle phenomena that emerge from the full ensemble, such as the zero resistivity that occurs at low temperatures in dense electronic systems where collisions should dominate, or the resistances that change by several orders of magnitude when some SCE materials are immersed in relatively small magnetic fields. The strong correlations between particles that are present when these phenomena occur render the one-particle approximation useless, and more sophisticated approaches are needed to rationalize the properties of these materials. Understanding, controlling, and predicting the emergent complexity of correlated-electron systems is one of the most pressing challenges in condensed matter physics at present. The rich phase diagrams of these materials, to be described below, make them natural candidates for devices where nonlinear responses can be exploited.

Surprises in the field of SCE research abound. Consider, for instance, the recent explosion of interest in the study of the iron-based layered superconductors known as the pnictides [5,6]. The main efforts to increase the record critical temperatures of layered copper oxides have been traditionally focused on the right-hand side of the $3d$ row of the periodic table where Cu is located. Iron (Fe) is in the middle of that row, and it is usually mainly associated with ferromagnetism, not with superconductivity. However, for reasons that are still still unclear, electrons in layers of Fe and As produce an unexpected superconducting state with a high critical temperature of approximately 50 K [6]. While fair it is to say that it is not yet totally clear whether these Fe-based superconductors are indeed part of the correlated-electron family, since the parent undoped compounds are simultaneously magnetic and metallic, as opposed to magnetic and insulating as in the cuprates, evidence is accumulating that the superconductivity is unconventional and perhaps mediated by spin excitations. Some investigations suggest that pnictides are located at *intermediate* on-site Coulombic repulsion couplings, in between the weak and strong limits [7].

6 A brief introduction to strongly correlated electronic materials

On the theory side, it is difficult to carry out reliable calculations for SCE materials, as explained in the introduction. Standard *ab-initio* methods do not properly incorporate correlations and often lead to metallic states for cases where a Mott insulator is the true ground state. In the absence of reliable *ab-initio* methods, a widely used theoretical approach to SCE materials is based on model Hamiltonians, since they seem to better capture the essence of correlated systems. However, as mentioned before, these models are still very difficult to solve accurately particularly using analytic techniques. For these reasons, it is not surprising that computational studies of complex systems in general, and correlated electrons in particular, are becoming a widely followed path to gather information about models, and this avenue has already led to considerable progress in the area of strongly correlated electrons.

The importance of understanding how complex phenomena emerge from simple ingredients was identified as one of the challenges for the next decade in a recent study by the U.S. National Academy of Sciences that addressed the current status of condensed matter and materials physics [8]. Also, the Basic Energy Sciences Advisory Committee of the U.S. Department of Energy has identified five “grand challenges” for science in order to be able to control matter all the way to atomic and electronic levels [9]. Among these generic challenges is an understanding of how the remarkable complex properties of matter emerge from correlations of their atomic or electronic constituents. Without a doubt, controlling correlated electrons is at present one of the most crucial areas of research in condensed matter and materials science.

1.4 Control of correlated electrons in complex oxides

Among the fundamental parameters for controlling the behavior of correlated electrons are (1) the tunneling rate for electron-hopping between atoms (typically regulated by a so-called hopping amplitude t , or by the one-electron bandwidth W which is linearly related to t) and (2) the density of charge carriers (or to be more precise, the band filling) [10]. The hopping amplitude t competes with the on-site electron–electron Coulomb repulsion energy U (also known as the Hubbard repulsion coupling U) and the outcome of this competition is the Mott transition, namely, an insulator–metal transition that often occurs in correlated-electron systems. As a function of the ratio U/t , the system undergoes several changes in the spin and charge arrangement and dynamics at low temperatures. In the limit of large U/t , every electron localizes on an atomic lattice site when the number of electrons precisely equals the number of those atomic sites (assuming just one active orbital per site in this example). In a Mott insulator, the ground state is often also spin antiferromagnetically ordered. But when U/t decreases and reaches some critical value, a transition to a metallic state occurs, as shown schematically in Figure 1.1. Another route to the Mott transition is by changing the filling (charge doping) of the correlated Mott insulator. Ideally, a tiny deviation from half-filling (or from an integer number of conduction electrons per atomic site in the d -electron system) should be sufficient to induce a transition to a paramagnetic metallic state, with a divergently large effective mass of conduction electrons. In most actual cases, however, a small but finite amount of filling change (i.e. doped charge) is necessary to stabilize a metallic state, free of the self-localization of conduction carriers caused by interactions with the lattice, spins, and the influence of disordering effects.

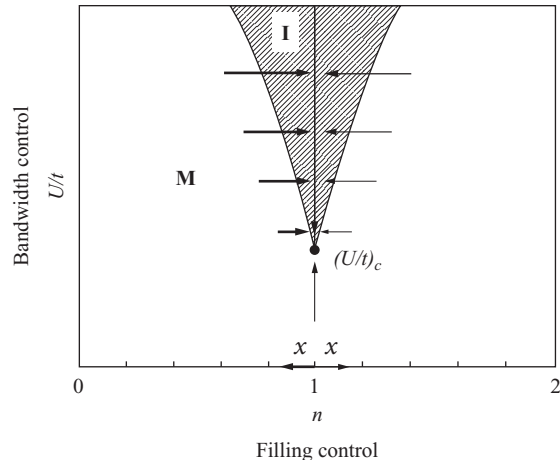


Fig. 1.1 Sketch of the generic low-temperature insulator (I) to metal (M) transition found in correlated-electron systems that are controlled by the bandwidth W (or equivalently by the hopping amplitude t) or the band filling n (doping x). U is the on-site Coulomb repulsion interaction, and $(U/t)_c$ represents the critical value where the transition occurs.

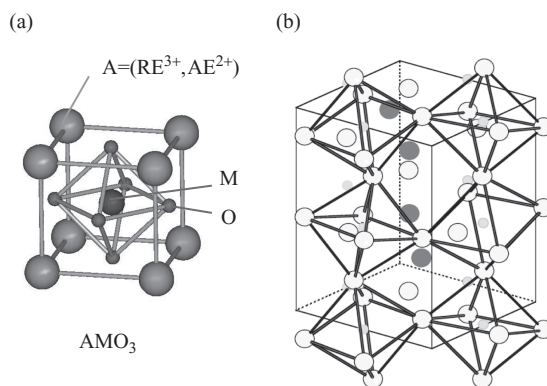


Fig. 1.2 (a) Perovskite structure of compounds with chemical formula $(\text{RE}, \text{AE})\text{MO}_3$, with trivalent (3+) rare-earth (RE) ions and divalent (2+) alkaline-earth (AE) ions located at the perovskite A-site, and the transition-metal element at the perovskite B-site. (b) Orthorhombically distorted (GdFeO_3 -type) structure of the perovskites.

These fundamental, and other related parameters in correlated-electron oxides, can be well controlled typically by the crystal engineering of a perovskite with the formula $(\text{RE}, \text{AE})\text{MO}_3$ (Figure 1.2 (a)), where RE, AE, and M represent the trivalent rare-earth ions, the divalent alkaline-earth ions (which can be in solid solution), and the transition-metal element, respectively. The ideal perovskite (AMO_3) exhibits a simple cubic structure, but the lattice distortions (Figure 1.2(b)), usually referred to as GdFeO_3 -type distortions, are governed by

8 A brief introduction to strongly correlated electronic materials

the size mismatch of the ionic radii of the A and M elements, or by the so-called tolerance factor f , defined as

$$f = (r_A + r_O) / \sqrt{2}(r_M + r_O), \quad (1.1)$$

where r_i ($i = A, M$, or O) represents the ionic size of each element i . When f is close to 1, the cubic perovskite structure is realized. As r_A , or equivalently f , decreases, the lattice structure transforms, first to the rhombohedral and then to the orthorhombic (GdFeO₃-type) structure, in which the M-O-M bond is bent and its angle deviates from 180°. This bond-angle distortion decreases the one-electron bandwidth W , because the effective d -electron transfer amplitude t between the neighboring M sites is governed by d -electron hybridization with the intervening O 2p state. The impact of the variation in W varying r_A is observed, for example, in the metal insulator transition in the family RENiO₃ [11]. In fact, LaNiO₃, with a maximum tolerance factor ($f \approx 0.96$) close to unity, is a paramagnetic metal with one conduction d electron per Ni atom, whereas other RENiO₃ materials with smaller f values (or decreasing RE ionic size) exhibit antiferromagnetic insulating ground states and undergo a thermally induced insulator metal transition (IMT) with increasing temperature.

Another important advantage of perovskites or related structures (e.g. layered structures, termed the Ruddlesden–Popper series) is the ease of chemical control of the band filling. Using the solid solution RE_{1-x}AE_x at the perovskite A site (AMO₃, see Figure 2(a)), the effective valence of the transition metal (M) becomes $3 + x$. In analogy to doped semiconductors, the increase (decrease) of x is customarily called “hole doping” (“electron doping”). These changes in x reflect a decrease (or increase) of the band filling or of the chemical potential.

A well-known example of a band-filling- (doping-) controlled Mott transition is the case of copper oxide high-temperature superconductors, such as La_{2-x}Sr_xCuO₄, in which the effective Cu²⁺ valence state, or more correctly the [Cu-O]⁰ state, is doped with holes and becomes a Cu^{(2+x)+} ([Cu-O]^x) state. It is well known that after the insulator to metal transition, that occurs at around $x = 0.06$, the ground state becomes superconducting [12, 13]. Another prototypical example is La_{1-x}Sr_xTiO₃, where hole doping of $x \approx 0.05$ drives the ground state from an antiferromagnetic Mott insulator to a paramagnetic metal with a high carrier density (band filling $n = 1 - x$), but with a large enhancement of the carrier mass, as compared to the calculated band mass [14].

Figure 1.3 presents a schematic of the overall electronic phase diagram of RE_{1-x}AE_xTiO₃ under the control of both the one-electron bandwidth W and the band filling (i.e. $1 - x$) in terms of varying the RE ionic radius and doping level x [15]. The “undoped” Mott insulator, for example La_{1-y}Y_yTiO₃, shows an increasing charge gap (Mott–Hubbard gap) with decreasing W (or increasing U/W), whereas the antiferromagnetic order turns to ferromagnetic through the influence of orbital ordering (to be discussed in more detail below). The critical doping level of the insulator-metal transition is increased from $x_c \approx 0.05$ for La_{1-x}Sr_xTiO₃, with a maximum W value (W_{La}), up to $x_c \approx 0.4$ for Y_{1-x}Ca_xTiO₃, with a relatively small W value (about 80% of W_{La}). The rather high concentration of holes needed to realize the metallicity of the small- W systems, such as Y_{1-x}Ca_xTiO₃, is common in the 3d transition-metal oxides with perovskite-like structures. There should be short-range/long-range polaronic ordering in such a highly doped insulating ground state, because of the combined effect of strong electron correlation and electron–lattice coupling. The charge–orbital ordered insulating state

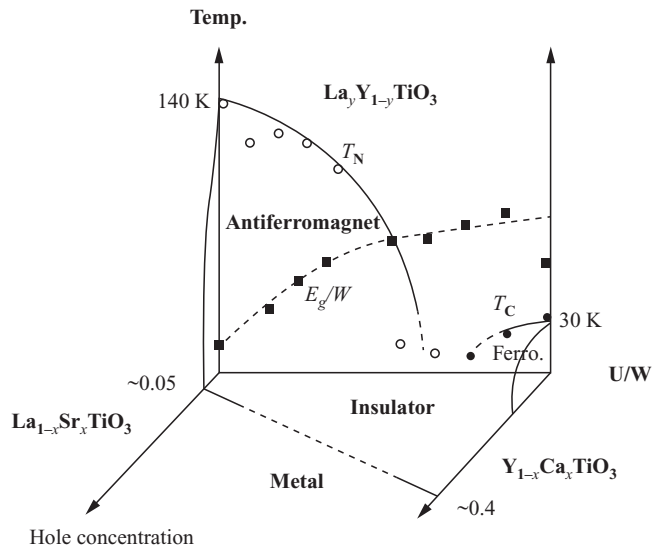


Fig. 1.3 Metal–insulator phase diagram of $\text{RE}_{1-x}\text{AE}_x\text{TiO}_3$ [14, 15]. In the end plane (temperature versus electron correlation U/W) with $x = 0$, the antiferromagnetic (T_N) and ferromagnetic (T_C) transition temperatures are plotted for the $\text{RE}=\text{La}_y\text{Y}_{1-y}$ system, where the variation of the normalized Mott–Hubbard energy gap (E_g/W) is also shown.

in the perovskite manganites is one such example where the state changes substantially when subjected to an external stimulus such as a magnetic field, electric field, or light irradiation, as described in the following sections.

Figure 1.3 also illustrates a typical characteristic of materials belonging to the correlated electron family. By varying the bandwidth, electronic concentration, and temperature, a rich variety of interesting phases can be stabilized. These phases present quite different properties, such as behavior like a metal or insulator in transport, or being antiferromagnetic versus ferromagnetic with regard to the spin order at low temperatures. The appearance of quite different tendencies in the same material by varying the above-mentioned parameters is typical of SCE systems. Figure 1.4 illustrates a similar qualitative behavior but for the cases of (a) Ru-oxides such as $\text{Ca}_{2-x}\text{Sr}_x\text{RuO}_4$ (known as the “ruthenates”) [2, 16], (b) Mn-oxides such as $\text{Nd}_{1-x}\text{Sr}_x\text{MnO}_3$ (known as the “manganites”, to be extensively discussed below in this chapter) [17], (c) the famous high temperature superconductors based on copper (the cuprates) including both hole and electron doping [13], and (d) the Co-oxides such as Na_xCoO_2 [18]. Future work will clarify if the new Fe-based superconductors (the pnictides) are located at strong or intermediate couplings, but they are already known to display a competition between magnetic and superconducting phases [5, 6, 7]. The phenomenon of presenting a very rich phase diagram has considerable importance particularly when close to the boundaries between phases, since a state with characteristics quite different from those of the ground state (say, a metal) may be located close in energy to the actual ground state (say, an insulator). As a consequence, small “perturbations” such as those introduced by relatively small external fields may unbalance

10 A brief introduction to strongly correlated electronic materials

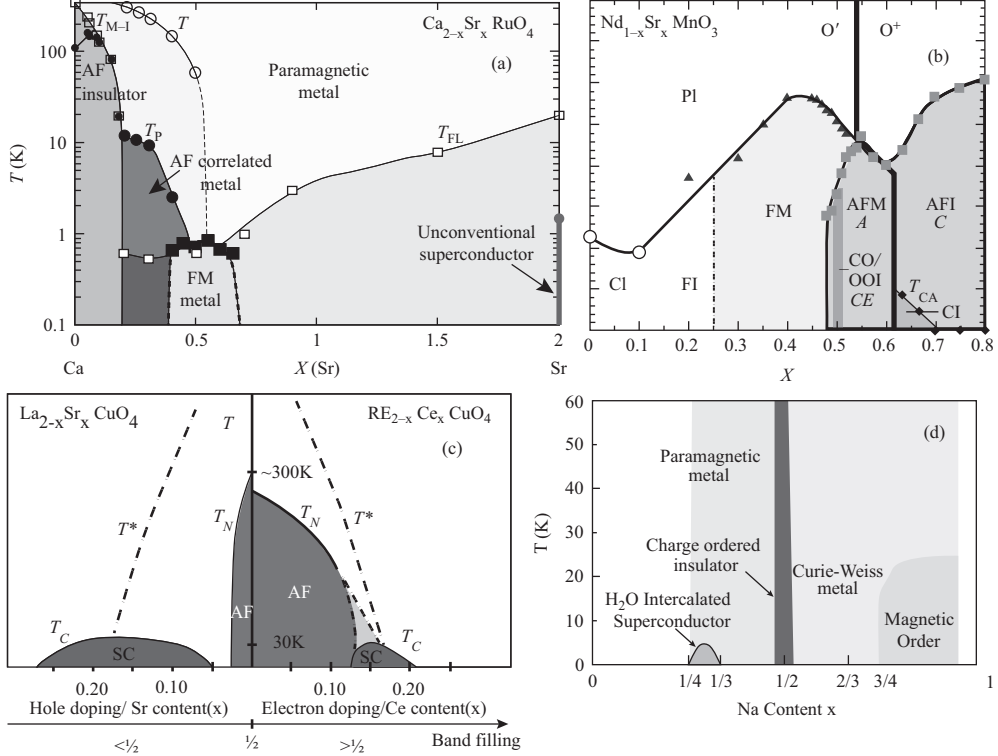


Fig. 1.4 (a) Phase diagram of $\text{Ca}_{2-x}\text{Sr}_x\text{RuO}_4$, a member of the family of compounds known as the ruthenates, reproduced from [2, 16]. Note the remarkably quite different properties obtained in this system by varying the temperature T as well as bandwidth W via the chemical substitution of Sr with Ca. The material can display properties corresponding to a good metal (paramagnetic metal) or a magnetically ordered metal (AF correlated metal and FM metal), or in a narrow range of temperatures, even a superconductor for 100% Sr. (b) Phase diagram of $\text{Nd}_{1-x}\text{Sr}_x\text{MnO}_3$, a member of the family of compounds known as the manganites, which display colossal magnetoresistance. Varying the concentration of holes x , via chemical substitution of Sr for Nd, the material presents, at low temperatures, a variety of metallic (ferromagnetic) and insulating (antiferromagnetic and ferromagnetic) phases. For details and a better description of the many phases see [17]. (c) Phase diagram of the hole-doped $\text{La}_{2-x}\text{Sr}_x\text{CuO}_4$ and electron-doped $\text{RE}_{2-x}\text{Ce}_x\text{CuO}_4$ high critical temperature cuprates, showing the antiferromagnetic insulating and superconducting phases, as well as other characteristic temperatures such as T^* which defines the pseudogap phase [13]. (d) Phase diagram of Na_xCoO_2 , reproduced from [18]. Note the presence of several very different phases, such as a superconducting phase, a magnetic regime, and a prominent charge-ordered state at $x = 1/2$. (c) Reprinted with permission from [13]. Copyright 2010 by the American Physical Society. (d) Reprinted with permission from [18]. Copyright 2004 by the American Physical Society.

the ground state and transform it into a quite different new ground state. This nonlinear effect of “perturbations” that are naively considered to be small a priori has profound implications for possible applications of these materials in actual devices.

1.5 Ordering of charge, spin, and orbital degrees of freedom

Consider a transition-metal ion (M) in a crystal with a perovskite structure. M is surrounded by six doubly negative oxygen ions (O^{2-}) which produce a crystal field potential that partly lifts the degeneracy of the d -electron levels (Figure 1.5). To understand this effect, simply consider the electronic wave functions. Those pointing towards the negatively charged O^{2-} ions ($d_{x^2-y^2}$ and $d_{3z^2-r^2}$, called e_g orbitals) must have higher energy than those pointing between the ions (d_{xy} , d_{yz} , and d_{zx} , called t_{2g} orbitals). In the Mott insulating state, almost all of the d electrons are localized on their respective atoms, making the spin and orbital degrees of freedom simultaneously active. The combination of these degrees of freedom produces a variety of complex spin-orbital ordering patterns. Prototypical cases are shown in Figure 1.6 for perovskites of LaVO_3 and YVO_3 , which are t_{2g} electron systems, and LaMnO_3 and BiMnO_3 , which are e_g electron systems.

In LaVO_3 , for example, the antiferromagnetic spin ordering with ferromagnetic chains along the z direction is known to induce an orbital-ordered state with alternate occupancy of d_{yz} and d_{zx} in the x , y , and z directions, in addition to the commonly occupied d_{xy} orbital [19] (in Figure 1.6 (a), the d_{xy} orbital on each V site is omitted for clarity). In spite of its nearly cubic character, the electronic structure is highly anisotropic because of the spin-orbital ordering. On the other hand, in YVO_3 [19] (Figure 1.6(b)), with a larger orthorhombic (GdFeO_3 -type) lattice distortion, staggered spin order and a d_{yz} or d_{zx} orbital-ordered state along the z axis are known to exist in the ground state. Thus, the relationships between the spin and orbital orders for these two compounds are exactly opposite, indicating the strong coupling between the spin and orbital degrees of freedom.

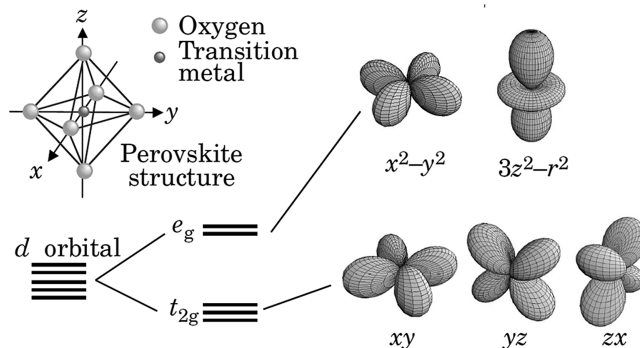


Fig. 1.5 Sketch illustrating how orbitals that are degenerate at the atomic level are split in a crystal field environment. Shown are the d -electron quantum mechanical orbitals and their level splitting in the octahedral coordination of O^{2-} .

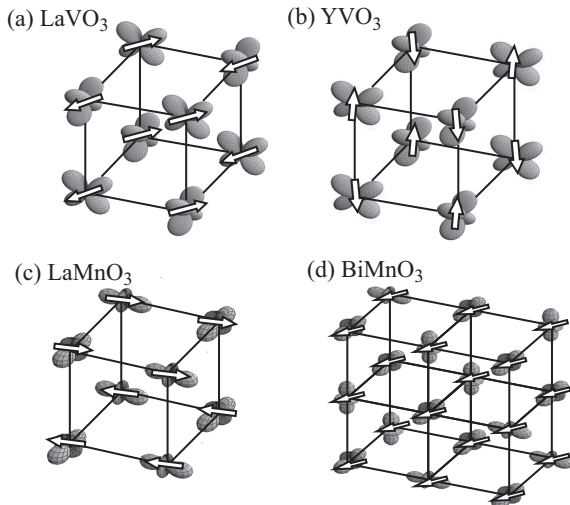


Fig. 1.6 The spin and charge ordering of the d electrons in (a) LaVO_3 [19], (b) YVO_3 [19], reprinted with permission from [19]. (c) LaMnO_3 [20], and (d) BiMnO_3 [21], all with (distorted) perovskite structures. (a) and (b) reprinted with permission from [19]. Copyright 1996 by the American Physical Society. (c) Reprinted from [20], with permission from Elsevier. (d) Reprinted with permission from [21]. Copyright 2002 by the American Physical Society.

In the perovskite manganites, the orbital degeneracy is easily lifted by coupling with the local deformation of the MnO_6 octahedron (called the Jahn–Teller effect), such as the elongation or compression of the octahedron along the c axis, compensated by compression or elongation along the a and b axes to keep the volume constant, favoring the occupation of the $d_{3z^2-r^2}$ and $d_{x^2-y^2}$ orbitals. Therefore, orbital ordering coupled with the collective Jahn–Teller distortion first emerges with decreasing temperature, and then regulates the spin ordering pattern at lower temperatures. In LaMnO_3 , a local linear combination of the $d_{3z^2-r^2}$ and $d_{x^2-y^2}$ orbitals produces orbital states elongated along the x and y axes, which alternate on the Mn sites in the ab (xy) plane, as shown in Figure 1.6(c). In this case, the Jahn–Teller distortion produces a macroscopic lattice strain, compressing the c axis and expanding the ab plane. The spins couple ferromagnetically on the ab plane, whereas they are stacked antiferromagnetically along the c axis, producing the so-called A-type layered antiferromagnetic state [20]. In BiMnO_3 , with a lower crystal symmetry because of the lone-pair on Bi^{3+} (Figure 1.6(d)), the complex orbital order can give rise to a Mott insulating ferromagnetic ground state [21].

In some relatively common cases, the compound remains electrically insulating or marginally metallic over a broad range of band fillings, in which a periodic array of doped holes or electrons appears. This phenomenon is called charge ordering. Figure 1.7 exemplifies several cases of such charge ordering in some quasi-two-dimensional transition-metal (M) oxides with chemical formula $(\text{RE},\text{AE})_2\text{MO}_4$, with the K_2NiF_4 -type structure (Figure 1.7(a)). In the isolated MO sheet of this crystal form, the spin, charge, and/or orbital tend to form

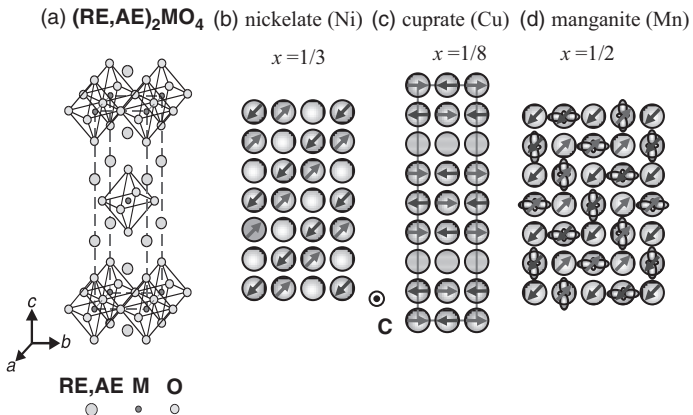


Fig. 1.7 Charge order in the form of “stripes” in hole-doped two-dimensional metal oxide sheets of layered perovskite materials with (a) K_2NiF_4 -type structure; (b) $La_{2-x}Sr_xNiO_4$ ($x \approx 1/3$) [22], (c) $La_{2-x}Ba_xCuO_4$ ($x \approx 1/8$) [23, 24], and (d) $La_{1-x}Sr_{1+x}MnO_4$ ($x \approx 1/2$) [25]. This figure is reproduced in color in the color plate section.

“stripes”, namely the extra charge (or in their absence, the extra holes) self-organize into quasi-one dimensional arrays. In $\text{La}_{2-x}\text{Sr}_x\text{NiO}_4$ (Figure 1.7(a), with RE = La and AE = Sr), for example, the hole doping, x , in the parent Mott insulator La_2NiO_4 cannot induce the insulator-metal transition up to $x = 0.9$ and instead forms a charge (hole) and spin stripe pattern running parallel to the diagonal direction of the NiO_4 squares (“diagonal stripe”), that is, along (110) in the tetragonal lattice [22]. At $x = 1/3$, in particular, the charge and orbital stripe state is the most stable, as shown in Figure 1.7 (b). This clearly illustrates that doping a Mott insulator does not always lead to a metal.

A similar hole stripe is also known to exist in some of the high-temperature superconducting copper oxides, as exemplified in Figure 1.7(c) for the $x = 1/8$ hole-doped La_2CuO_4 [23, 24]. In this case, the one-quarter-filled (i.e. 50% hole-doped) stripes run along the (100) or (010) directions (“horizontal or vertical stripes”) in the half-filled CuO_2 background. The incommensurate spin order observed in the underdoped region (say, $x < 0.12$) of La_2CuO_4 might originate from this exotic charge order. Reflecting the one-quarter-filled nature of the vertical/horizontal stripes, the electrical conduction along these stripes appears to survive and manifests itself as a one-dimensional charge dynamics and Fermi-surface structure.

Even more complex features arise in the doped manganites as a consequence of the close interplay among the spin, charge, orbital, and lattice degrees of freedom, as exemplified in Figure 1.7(d) for hole-doping levels of $x = 1/2$ [25]. In a classical picture, Mn^{4+} (with three t_{2g} electrons as the local $S = 3/2$ spin) and Mn^{3+} (with the $S = 3/2$ local spin plus one e_g electron) should coexist (more details are provided in the next section). The charge ordering shows a checkerboard pattern, whereas the orbital on the same Mn^{3+} sites shows the larger unit-cell ordering with approximately alternating $d_{3x^2-r^2} - d_{3y^2-r^2}$ (or $d_{y^2-z^2} - d_{z^2-x^2}$) orbital occupancy. The observed spin ordering pattern arises from the subtle compromise between the

14 A brief introduction to strongly correlated electronic materials

antiferromagnetic superexchange interaction among the t_{2g} local spins and the ferromagnetic double-exchange interaction (also to be addressed in more detail below) mediated by the e_g electron hopping between the Mn^{3+} and Mn^{4+} sites. The orbital ordering regulates the anisotropic e_g electron hopping, and hence, the Mn^{4+} sites adjacent to the lobe of the e_g orbital on the nearest Mn^{3+} site are linked through a ferromagnetic interaction. As a result, interesting ferromagnetic “zigzag” chains appear along the diagonal direction in the ground state. These complex forms of charge–orbital–spin ordering are ubiquitous in the highly (moderately) doped nonmetallic manganese oxides with perovskite-related structure.

1.6 Model Hamiltonians

In several transition-metal oxides, particularly those in the middle of the $3d$ row of the periodic table, there are two effectively separated electronic degrees of freedom originating from the same ion. Figure 1.8(a) illustrates, similarly to the explanation for Figure 1.5, the case of the Mn oxides where the lattice environment splits the originally five-folded degenerate $3d$ orbitals into two e_g levels and three t_{2g} levels. The valence of Mn in, e.g. LaMnO_3 is 3+, and, consulting the periodic table, this immediately shows that four electrons must be accommodated in the active five $3d$ levels. In practice, the crystal field splitting between these levels is not sufficiently large to prevent Hund’s rule of atomic physics from dominating and, as a consequence, the e_g levels carry one electron while the three other electrons are located into the t_{2g} levels, and they all orientate their spins in the same direction. This effectively creates a separation between the electrons at the e_g levels, that become mobile after hole-doping is introduced via the replacement of La by Sr or Ca, and the well-localized spins residing at the t_{2g} levels that are

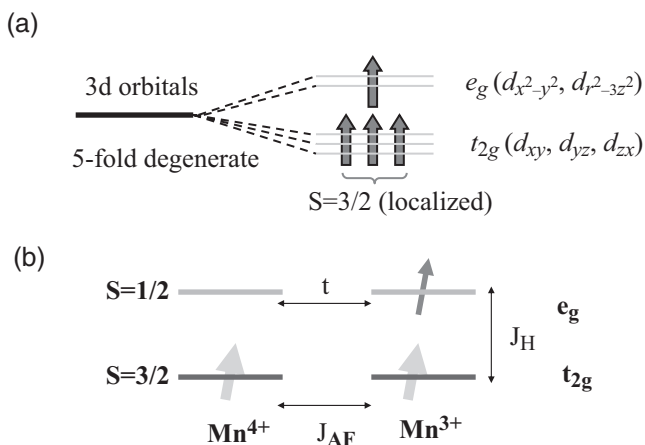


Fig. 1.8 (a) Sketch illustrating the splitting of levels in a manganese ion due to the crystal field, and the effective formation of two types of degrees of freedom: mobile e_g electrons and localized t_{2g} spins (with a sufficiently large total spin that they are often approximated by a classical spin). (b) Sketch illustrating some of the interactions that appear in model Hamiltonians for manganites, as well as the double-exchange mechanism for ferromagnetism in these compounds.

not affected by chemical doping in the ranges usually studied. In addition, it has been shown that a t_{2g} spin value of 3/2 can be considered to be large enough to approximate those t_{2g} spins by classical spins. Thus, effectively there is an intriguing coexistence of quantum itinerant and quasi-classical localized degrees of freedom in these materials. This separation is important for many reasons. In particular, it provides a procedure to carry out computational studies of model Hamiltonians for Mn oxides [26].

After establishing the effective separation between mobile and localized degrees of freedom at each Mn ion, bringing two of those Mn ions together illustrates the typical interactions that need to be incorporated into model Hamiltonians to properly describe their physics. Figure 1.8(b) shows schematically the previously discussed spin 1/2 and 3/2 degrees of freedom of a manganese ion in valence state 3+, together with another manganese that has lost the e_g electron (due to the influence of chemical doping) and is now in a valence state 4+. With regard to the mobility of the e_g electrons, a “hopping” term for those electrons must be incorporated to account for the tunneling of an e_g electron from one Mn to the other (in this approximation the intermediate oxygen merely acts as a bridge). The amplitude for this process to occur is t . In addition, the localized spins 3/2 can interact like any pair of localized spins via a Heisenberg interaction which is regulated here by a coupling called J_{AF} . At each manganese ion, the Hund rule is enforced by including a ferromagnetic term that links the spins of the localized and mobile electrons, with strength J_H . Finally, not shown in the figure but still very important, is the Jahn–Teller coupling of the electrons to the oxygen vibrations that can split the doubly degenerate e_g levels. The orientation of the spins in Figure 1.8 (b), with the two t_{2g} spins pointing in the same direction, illustrates the reason for the presence of a so-called “double exchange” ferromagnetic phase in these compounds: in order for the e_g electrons to be able to move easily and gain kinetic energy without expending an energy as large as the Hund coupling (\sim eV), the t_{2g} spins must be oriented ferromagnetically. This simple mechanism, that fails at large enough J_{AF} or e-phonon couplings, is, for historical reasons usually referred to as a double exchange.

To avoid technicalities in this introductory chapter, the actual mathematical form of the model Hamiltonian for manganites will not be explicitly presented here. Interested readers should consult [26] for details (or [12] for models for the cuprates). In [26], a description of the phase diagrams of these models for manganites can also be found, as well as several references and a description of the many-body techniques used to obtain those phase diagrams. Typically they are complex, presenting many phases with competing tendencies involving metals and insulators, and a variety of spin, charge, and orbital orders, similar in several respects to the phase diagrams of the real materials shown in Fig. 1.4.

1.7 Intrinsically inhomogeneous states

A variety of experimental probes and theoretical calculations aimed at understanding materials of the strongly correlated electron family have consistently unveiled a tendency to form states that are not homogeneous, in the sense that rather different spin, charge, and orbital arrangements can coexist in the same sample [2, 26, 27]. It appears that these tendencies originate in the competition between the several phases that are close in energy in some SCE materials. These issues have attracted considerable attention, particularly in the context of the manganites and the cuprates. In manganites, early Monte Carlo and dynamical mean field calculations revealed

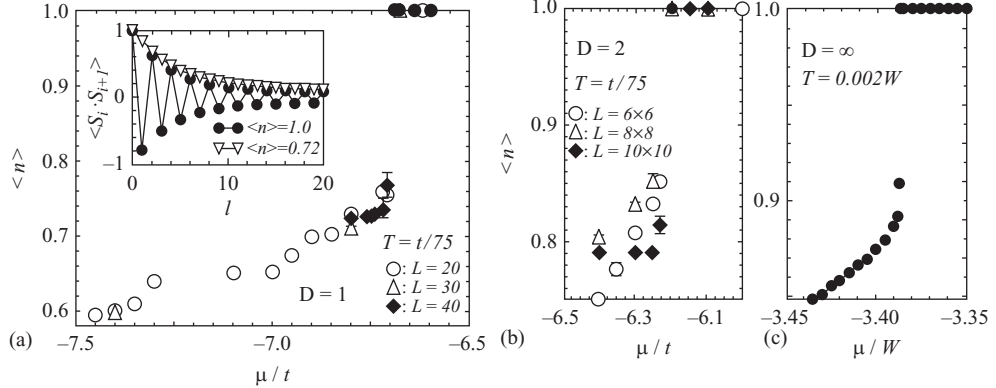


Fig. 1.9 Electronic density $\langle n \rangle$ of the e_g electrons versus chemical potential, reproduced from [27]. These results were obtained via a Monte Carlo simulation of models for manganites, involving an Exact Diagonalization of the fermionic sector and Monte Carlo sampling of the classical spins [27]. The left panel was obtained in one dimension and it shows a clear discontinuity in the curve, signaling the presence of unstable density regions where phase separation occurs [27]. The middle panel are similar results but for two dimensions. The right panel illustrates similar physical results, but using the dynamical mean-field approximation that is exact at infinite dimensions. For more details see [26, 27, 28].

a tendency towards a phenomenon called phase separation [26, 27, 28]. This manifests itself as a discontinuity in the curve electronic density $\langle n \rangle$ versus chemical potential [27], as shown in Figure 1.9. In this regime, a cluster that is nominally prepared at an electronic density $\langle n \rangle_{\text{nom}}$ which is not allowed, e.g. a density in the discontinuity range between 1.0 and ~ 0.78 , if Figure 1.9 (a) is considered, will spontaneously separate into two regions with densities at the extremes of the jump, each occupying a volume in the proper proportion such that the average density is $\langle n \rangle_{\text{nom}}$. A crude sketch of this phenomenon is shown in Figure 1.10(a), where the white and gray tones indicate the two macroscopic regions involved in the process, with different electronic densities. However, note that such a phase-separated state cannot be stable because there is a macroscopic separation of charge that is not balanced (the positive ions that keep the ensemble neutral are not mobile enough to migrate and compensate for the electronic charge separation). When the Coulombic $1/r$ long-range interactions are taken into account in the calculations, then complex inhomogeneous states are typically formed involving, for example, bubbles of one state embedded into the other, or striped arrangements as previously discussed (see Figures 1.10 (b) and (c)), with typical characteristic lengths in the nanometer scale region. This whole phenomenon is sometimes referred to as “electronic phase separation” and it was first widely discussed in the context of the cuprates, to rationalize the appearance of the stripes [23, 24]. In manganites, inhomogeneous states have also been widely reported [26, 28]. Thus, in both manganites and cuprates, a variety of calculations and experiments suggest that this tendency to separate into two states at the nanometer scale must be seriously considered. Readers interested in this popular subject should consult [23, 24, 26, 28] and the cited literature therein for details.

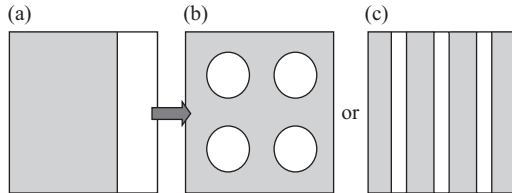


Fig. 1.10 Qualitative sketch of a macroscopically phase-separated state (a), where the gray and white regions represent two phases of the same compound but with different electronic densities. (b) and (c) represent possible nanometer scale arrangements of these phases obtained after proper consideration of the long-range $1/r$ Coulomb repulsion between the electrons. This figure is reproduced from [28] where more details can be found. Reprinted from [28] with kind permission from Springer Science+Business Media.

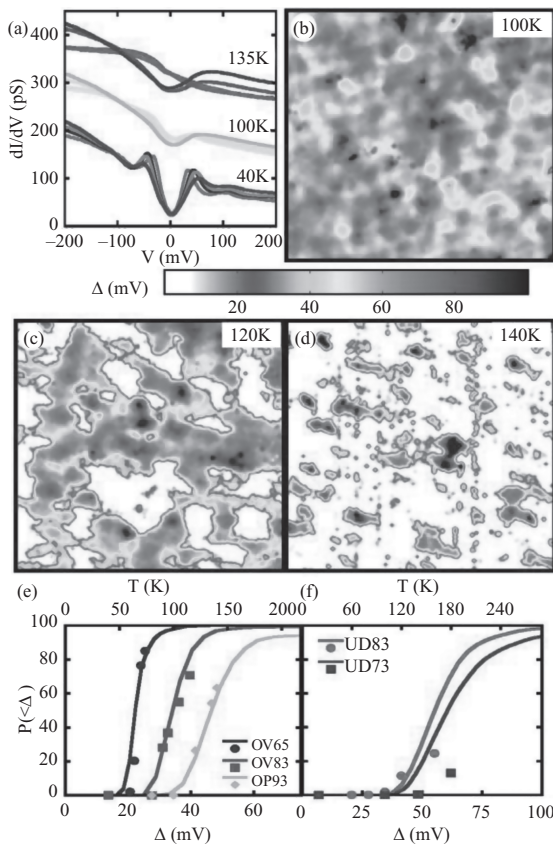


Fig. 1.11 Example of an experimental result that illustrates the presence of inhomogeneous states in a transition-metal oxide. Shown are results reported in [29], containing scanning tunneling microscopy (STM) data gathered for a high-temperature superconductor material with a critical (optimal) temperature of 93 K. The colored regions have a d -wave STM spectrum, and the remarkable result is that these superconducting areas are observed even at temperatures as high as 120 K, well above the critical temperature, contrary to the behavior of typical BCS low-temperature superconductors. Reprinted by permission from Macmillan Publishers Ltd [29], copyright 2007. This figure is reproduced in color in the color plate section.

Recently, Scanning Tunneling Microscopy (STM) experiments have revealed a variety of interesting inhomogeneous states that relate to the previous discussion. For instance, STM experiments for a high critical temperature superconductor [29] with a critical temperature $T_c \sim 93$ K revealed regions where the local density of states closely resembles that of a d -wave superconductor, but at temperatures considerable higher than T_c . Figure 1.11 contains some of these STM results. Note that at 120 K, namely almost 30 K above T_c , as much as half the sample still has local d -wave characteristics, which is a remarkable result. The d -wave regions have random shapes instead of stripes or other more uniform patterns. Some of the theoretical proposals for understanding these effects rely on the influence of quenched disorder over the competition between superconducting and antiferromagnetic states [30, 31].

1.8 Giant responses in correlated electron systems

The several competing tendencies in correlated-electron materials lead to rich phase diagrams, containing a variety of phases with spin, charge, and orbital order; superconducting states; metals and insulators; multiferroics, and other states (as discussed before, see Figures 1.3 and 1.4). These phases are interesting by themselves but, in addition, their presence in the same material suggests that the energies of each phase must be similar, since small changes in composition, temperature, pressure, external fields, and other parameters tend to induce a transition from one to another. These transitions are often of first order, which is natural for states with such different properties.

In several materials of the strongly correlated electron family, giant responses to external fields have been observed in the region of phase competition. A typical and widely studied example is the case of the colossal magnetoresistance (CMR) in manganites [32, 33]. At particular chemical compositions, these materials present a ferromagnetic metallic ground state, but they display unexpected resistivity versus temperature curves. The resistivity has insulating characteristics, namely it increases with decreasing temperature, above the ferromagnetic ordering temperature T_C , followed by a sharp peak at T_C upon cooling (sometimes involving a first-order transition, as discussed below), and finally it drops to a metallic state as the temperature is lowered further (see Figure 1.12 for the case of $\text{La}_{1-x}\text{Ca}_x\text{MnO}_3$). The shape of a typical CMR resistivity versus temperature curve is considered exotic because it is unusual to have an insulator as the high-temperature “normal” state of a low-temperature metallic ferromagnet. However, the most curious property is obtained by immersing the material into an external magnetic field of just a few Teslas. In this case, the resistivity peak is found to be rapidly suppressed, generating as a consequence a large and negative magnetoresistance effect, which was dubbed “colossal” magnetoresistance in the early days of its discovery in 1994 [32, 33]. Although technological applications of this effect in computer-read sensors will need T_C to be raised by a substantial factor to comfortably reach room temperature, nevertheless the CMR phenomenon already defines a fundamental science puzzle that many groups have been trying to decipher for several years.

Present understanding of the CMR effect is based on phase competition. Of the several manganites obtained by varying the trivalent and divalent ions in the chemical formula, only those with relatively small bandwidths show the most prominent CMR effect (the CMR effect in large bandwidth manganites is still present but with a reduced magnitude). Concomitant with a small bandwidth, insulating states that compete with the ferromagnetic metal are often found in

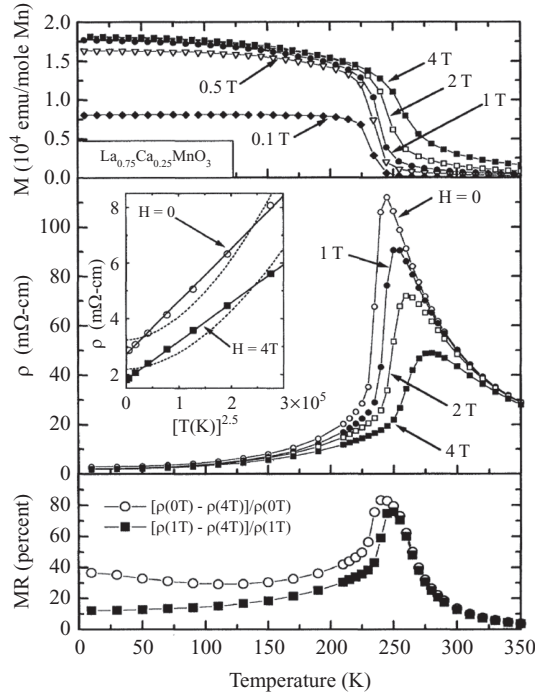


Fig. 1.12 Magnetization, resistivity, and magnetoresistance of the manganite $\text{La}_{0.75}\text{Ca}_{0.25}\text{MnO}_3$, as a function of temperature and for various magnetic fields, illustrating the presence of the CMR effect in this compound. Reprinted with permission from [33]. Copyright 1995 by the American Physical Society.

phase diagrams. The reason is that having a small bandwidth enhances the relative importance of electron–phonon couplings, and complex charge, orbital, and spin-order arrangements with overall insulating properties are found at low temperatures, as discussed earlier in this chapter.

Theoretically, it was argued early on that the region of phase competition between the ferromagnetic metal and the insulator is where CMR is found [26]. This hypothesis was confirmed by recent state-of-the-art computer simulations based on the double-exchange model for manganites, supplemented by a robust coupling to Jahn–Teller lattice displacements [34]. Some representative theoretical curves are shown in Figure 1.13. It is clear that these results, which were obtained using Monte Carlo simulations employing large computer clusters or even supercomputers, display resistivity curves that much resemble those obtained in experiments, including first-order characteristics in the CMR transition under some circumstances, such as when being in close proximity to the competing insulator in the clean limit. It can be said that the CMR effect has now been “trapped” in a box, in the sense that it appears in controlled numerical studies of small clusters of about 100 Mn atoms, and it is now up to theorists to “ask” the proper questions of the computers in order to understand qualitatively its origin at a deeper level.

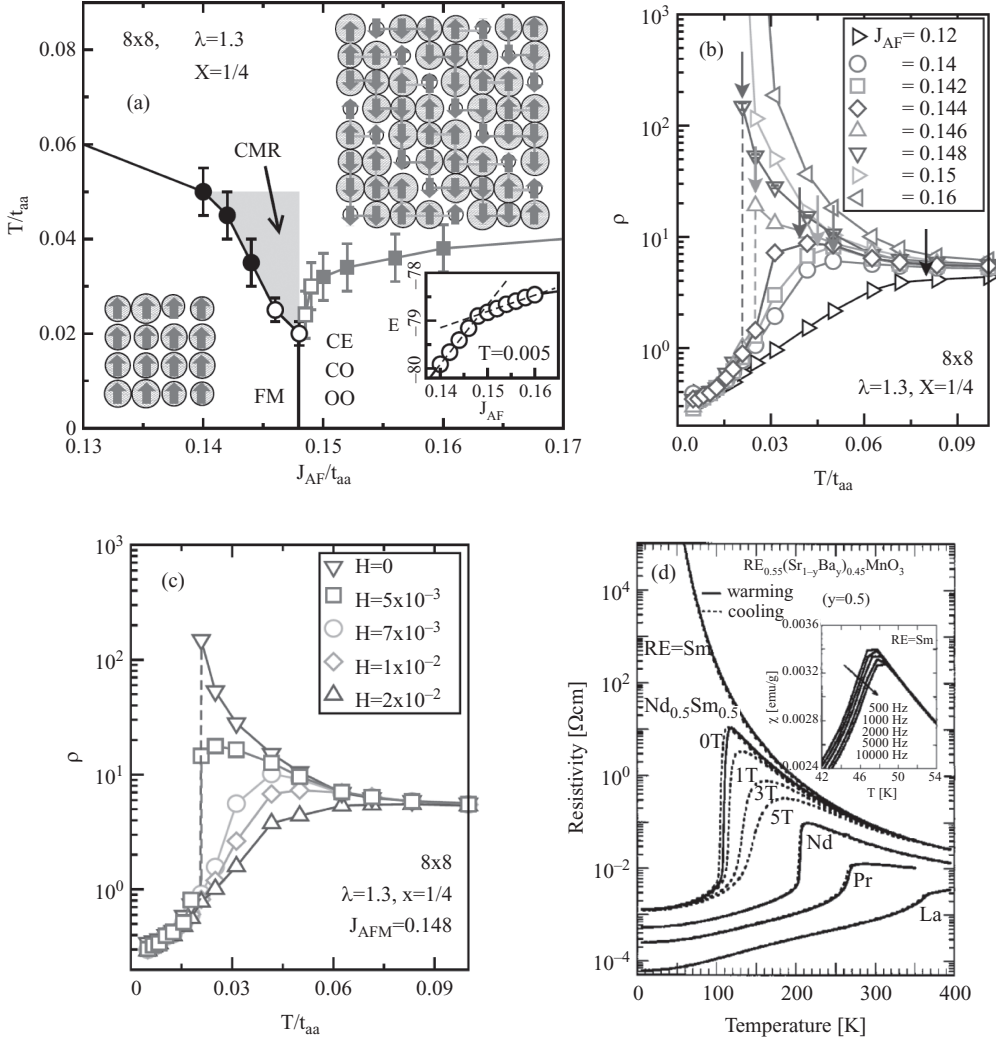


Fig. 1.13 Results of a computer simulation corresponding to a double-exchange two-orbital model for the CMR manganites, adapted from [34]. Shown here are computationally calculated resistivities versus temperature curves, parametric with the couplings in the model, as described in more detail in the original publication. (a) contains the phase diagram at hole doping $x = 1/4$, with the presence of two competing states (FM metal and CE/CO/OO insulator). The characteristic resistivity peak of materials exhibiting colossal magnetoresistance is observed in this study, see panel (b). In panel (c) the rapid reduction of the resistivity with increasing magnetic fields H is shown. Panel (d) contains experimental results [38] to illustrate how similar theory and experiment are.

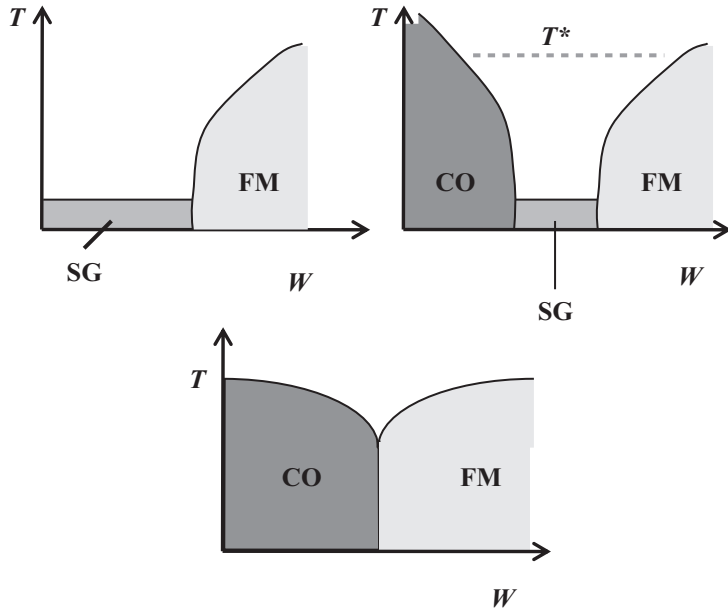


Fig. 1.14 Generic temperature (T)–bandwidth (W) phase diagram of manganites in the region of competition between the FM metallic state and a charge-ordered (CO) (typically also orbitally ordered (OO) and spin antiferromagnetic (AF)) insulator. The lower panel is the case of the “clean limit” without quenched disorder. Here the transition FM–CO is first order. The CMR effect can be observed, as shown in [34, 35], but only in a narrow region close to the FM–CO transition. The upper right panel illustrates the case of weak/moderate quenched disorder, where a spin-glass (SG) region is created in between the two competing phases. T^* is a remnant of the clean limit transitions, and it is the characteristic temperature where clusters of the competing phases appear upon cooling. The upper left panel corresponds to large quenched disorder, where the results of Figure 1.15 indicate that the CO phase disappears. For more details see [2, 26, 28, 36] and references therein.

The same theoretical/computational investigations that lead to Figure 1.13 have also suggested [34, 35] that in the insulating region above T_C the short-distance charge and spin order closely resemble those of the insulating state that competes with ferromagnetism. Perhaps induced by large entropy effects, at temperatures higher than T_C , the system behaves as though the insulator were the dominant state. However, T_C is where the energy prevails over the entropy, and the true metallic ground state is stabilized upon cooling. Moreover, it has been observed [26, 28, 34, 35] both theoretically and experimentally, that quenched disorder caused by chemical doping enhances the window in parameter space where these effects are observed. A schematic phase diagram, including both the bandwidth and disorder strengths, was predicted by theory and confirmed by experiments. In this phase diagram, shown in Figures 1.14 and 1.15, an original first-order transition is smeared by disorder, and it is in the intermediate region, which has glassy properties and mixed phase characteristics, where the colossal effects can be observed [36].

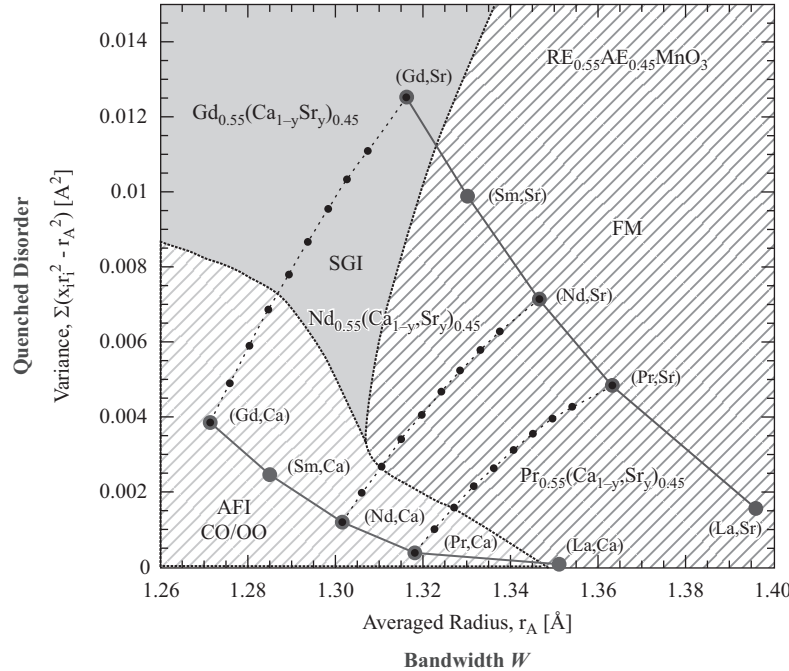


Fig. 1.15 Experimental phase diagram of manganites obtained by varying the bandwidth W and quenched disorder strength (variance). Note the presence of three regimens: the FM metallic phase induced by double exchange, the CO insulating phase (also OO and AF), and a spin-glass insulator (SGI) induced by quenched disorder. Figure adapted from [38].

Let us discuss in more detail Figure 1.13 which illustrates the exciting results obtained in recent calculations, where the properties of the double-exchange model for manganites were studied using computational techniques (more specifically, the Monte Carlo technique supplemented by the Exact Diagonalization method for the e_g electronic sector [27, 34, 35, 37]), employing a small cluster with only 64 manganese sites. These small clusters may seem indeed very tiny compared with the huge number of atoms in a real material. However, it has been extensively shown, via a variety of examples, that the qualitative aspects of the physics of these model Hamiltonians can still be captured, at least qualitatively, using small systems with about 100 active sites (unless very subtle properties such as critical exponents near critical temperatures are needed). Shown in Figure 1.13 (a) is the phase diagram of the analyzed model, varying the coupling J_{AF} among the localized spins and the temperature T , at a fixed value of the electron–phonon coupling. For relatively small values of J_{AF} , the ground state at hole concentration $\frac{1}{4}$ (equivalent to $x = 0.25$ in the $\text{La}_{1-x}\text{Ca}_x\text{MnO}_3$ language) is ferromagnetic, as expected due to the double exchange mechanism discussed before in this chapter. However, increasing J_{AF} (or at a fixed J_{AF} increasing the electron–phonon coupling), eventually an insulating state is always reached, with a complicated pattern of charge, spin, and orbital order (see sketch in Figure 1.13(a)). But finding an insulating state that is competing with the

ferromagnetic metallic state is not the main result. Much more important is the behavior of the resistivity versus temperature in these small clusters, when tuning the J_{AF} coupling to be close to the transition from one phase to the other. Figure 1.13(b) shows typical examples. These results show that inside the FM phase and far from the region of competition, the curve is metallic as it should be. Reciprocally, inside the insulating phase, and also far from the competing phase, the curve is clearly insulating, as it should be. The surprises are in the middle: rather than simply switching from metal- to insulator-like resistivity curves by varying J_{AF} , there is a narrow range of couplings where, above T_C the resistivity is insulating (namely increasing with decreasing temperatures), but when T_C is reached upon cooling then a first-order (i.e. discontinuous) transition transforms the insulating-like behavior into a metal. Thus, in a narrow regime of couplings, the low-temperature ground state is FM and metallic, but the state above T_C much resembles that of the competing insulator. These results are in excellent agreement with experiments, such as those shown for instance in Figure 1.12.

Figure 1.13(c) contains the results when an external magnetic field is added. In this case, a rapid suppression of the resistivity can be observed, even for relatively small magnetic fields, producing a very large negative magnetoresistance similar to that observed experimentally (see Figure 1.12). Figure 1.13(d) contains experimental data showing how similar those results are when compared with theory [38]. In conclusion, via intensive numerical calculations (which use the resources of clusters of computers with hundreds of nodes, or supercomputers with thousands of nodes, see [34, 35]) the complex behavior of models for CMR manganites is starting to be unveiled, and thus far agreement with experiments is remarkable. So it is not difficult to imagine that similar techniques could also be used for the study of superlattices involving manganites, as described elsewhere in this book, bringing theory and experiments closer together in this promising area of research.

The giant nonlinearity with magnetic fields observed in CMR manganites, widely believed to originate in phase competition, is merely one example of the potentially enormous responses that several correlated-electron systems could display. In fact, the sketch in Figure 1.14 actually does not depend in any detail on the properties of the competing states, but only depends on the existence of the competition itself. Note, however, that if one of the phases is not ferromagnetic, then the external “perturbation” that triggers the giant response becomes less obvious than those generated by a uniform magnetic field as in manganites. In fact, recent investigations have suggested that giant responses could occur in underdoped cuprates as well. In this case, the external perturbation is conjectured to be due to the proximity to a well-developed superconductor, which may induce superconductivity in an otherwise non-superconducting underdoped cuprate [30], which is believed to contain superconducting clusters where the superconducting amplitude is developed but the phases between clusters are random. More generally, it might occur that the exotic properties of the famous pseudogap regime of the high-temperature superconductors could originate in phase competition between the parent compound, which is an antiferromagnetic insulator, and the superconducting state itself [30]. In addition, many other correlated-electron materials could potentially present similar exotic nonlinear responses to special perturbations. Surprises of this kind might be found in several compounds of the correlated-electron family.

Note that the nonlinearities described here tend to occur concomitantly with nanometer-length-scale inhomogeneities [2, 26, 28, 36]. For example, a variety of experiments in hole-doped manganites have shown convincingly that, in the CMR regime there are nanometer

24 A brief introduction to strongly correlated electronic materials

length-scale clusters with characteristics similar to those of the charge-ordered state that is stable at half-doping $x = 0.5$ in the LCMO phase diagram, even though the ground state at low temperatures at the values of x investigated is a ferromagnetic metal [26, 28]. Even before the experimental investigations in this context established these results, theoretical calculations had already predicted strong tendencies towards inhomogeneous states, a phenomenon widely known as phase separation, as previously described in this chapter. This kind of self-organization of electronic degrees of freedom also occurs in some high-temperature superconductors, and also in nickel oxides where states containing striped arrangements have been identified, as previously mentioned. As also discussed previously, experiments [29] have shown that other kinds of inhomogeneous states, with irregular patterns, could occur in Cu-oxide superconductors above the critical temperature (Figure 1.11).

1.9 Importance of quenched disorder and strain

A variable often overlooked in the consideration of the physics of materials, including correlated electron systems, is the strength of *quenched disorder* in the sample under study. This disorder may merely be caused by impurities or imperfections in the growing process. But it may be intrinsic as well, such as in the cases where chemical doping is needed to add or remove carriers from a particular material, such as when a trivalent ion is randomly replaced by a divalent ion. Not only do these two types of ions have different valences but they also have different sizes which tends to induce lattice distortions, as already discussed when addressing how the bandwidths of material can be altered by chemical substitution.

In the area of manganites, experiments for the case of $\text{Ln}_{1/2}\text{Ba}_{1/2}\text{MnO}_3$, which admits both ordered and disordered crystal forms with regard to the location of the Ln and Ba ions, have unveiled the profound influence of disorder on the properties of these materials (and by extension, in many other SCE compounds as well). Figure 1.16 shows the phase diagrams for both the ordered and disordered versions of this compound (for details see [39]). In the ordered case, a first-order transition separates the FM and CO/OO phases, similarly to Figures 1.13(a), 1.14, and 1.15 for the clean limit. However, in the disordered case, the Curie temperatures for ferromagnetism are substantially reduced, and a spin glass (SG) new phase is created between the FM and CO/OO phases (the latter not shown in the figure). Even more dramatic and crucial for the issues discussed here, are the transport properties of these two versions of the same material. Figure 1.16 shows that, while the ordered version has a standard insulating behavior, the disordered one actually presents the CMR effect. Thus in this case, experiments show that disorder is *needed* for giant nonlinear behavior to appear in these manganites. Presumably, the existence of nonlinearities originating in phase competition may be present in other similar compounds as well.

Also, Cu-oxide high-temperature superconductors may be influenced substantially by quenched disorder. Figure 1.17 contains a revised phase diagram recently proposed for the cuprates [40], including not only the canonical temperature and hole-doping variables, but also the strength of quenched disorder as a “new” axis. In this phase diagram, the material called YBCO corresponds to a fairly clean case, and in this situation the transition from the AF state to the superconducting phase appears to occur via a weak first-order transition or a quantum critical point (this issue is still under discussion). In the other extreme, some one-layer cuprates, such as the 214 compounds, have the strongest disorder and an intermediate spin glass phase

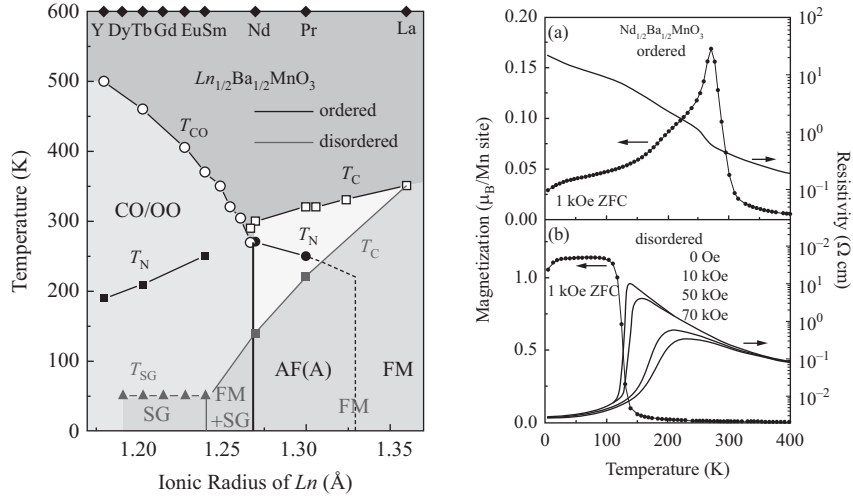


Fig. 1.16 (Left panel) Phase diagram for the A-site ordered (black symbols) and disordered (gray triangles and squares symbols) perovskites with half doping $\text{Ln}_{1/2}\text{Ba}_{1/2}\text{MnO}_3$, as a function of the ionic radius of Ln . CO/OO, FM, and SG are the charge/orbital ordered, ferromagnetic, and spin-glass states, respectively. Note that for the case of the A-site ordered compound, the CO/OO and FM phases are in contact and the critical temperatures are between 300 K and 500 K. However, in the disordered version, the critical temperatures are much reduced, the SG phase appears, and the CO phase has disappeared in the range of chemical doping investigated. (Right panel) Magnetization and resistivity of ordered and disordered $\text{Nd}_{1/2}\text{Ba}_{1/2}\text{MnO}_3$. Note that the A-site disordered material shows the CMR effect near the Curie critical temperature, while the ordered version does not, illustrating the importance of quenched disorder in this context. All these results are reproduced from [39] where more information can be found.

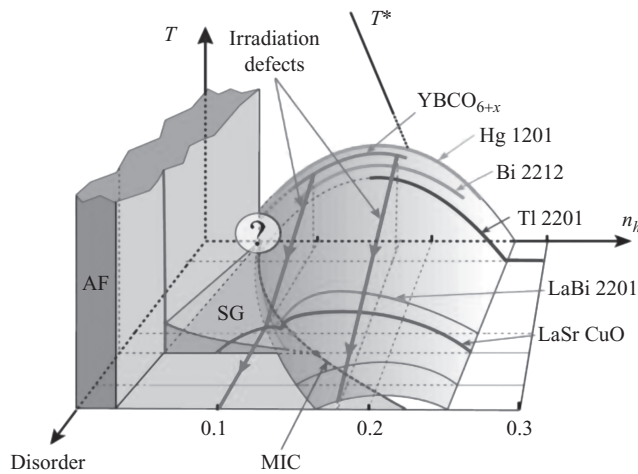


Fig. 1.17 Schematic phase diagram of the high-temperature superconducting cuprates as a function of temperature, hole doping n_h , and disorder strength, reproduced from [40]. Shown are: the AF phase in the undoped case, the superconducting phase upon doping, and the spin-glass (SG) state obtained by increasing the amount of disorder. These experimental results were obtained via resistivity measurements and with the disorder induced by electron irradiation [40].

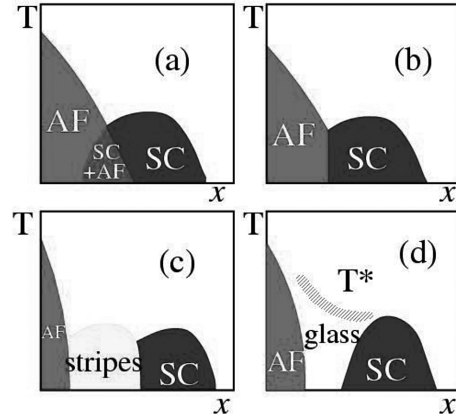


Fig. 1.18 Schematic phase diagram illustrating the possible ways in which an antiferromagnetic (AF) state can compete with a superconducting (SC) state (for details see [30, 31]). In panel (a), the transition from AF to SC states occurs via a region of homogeneous coexistence of both order parameters. In (b), a first-order transition separates both phases. In (c), a region with stripes made of the competing phases is located in between the competing states. These three cases (a,b,c) can be found in the clean limit [30, 31]. In (d), the modified phase diagram of (a) is shown after quenched disorder is introduced. In this case, a spin-glass phase is generated in between the AF and SC states, as in the widely discussed experimental phase diagram of the single-layer “214” cuprate compound. In this context, T^* is a remnant of the original clean-limit phase transitions. For additional details, the reader should consult [30, 31].

is formed, similarly to the case of manganites with disorder. Theoretical calculations [30, 31] using phenomenological models have suggested that the phase diagram of cuprates in the clean limit could have a region of uniform coexistence of AF and SC states, or a first-order transition separating those states, or even stripes made out of AF and SC phases. But it is only after quenched disorder is incorporated that a spin glass is formed and a new temperature scale T^* is obtained, a remnant of the original clean-limit phase transitions, reproducing the famous 214 phase diagram (Figure 1.18).

As a consequence, the possibility of producing doped materials in artificial superlattices via the transfer of charge from one component to another (for instance from LaMnO_3 to SrMnO_3 as in the cases described by Bhattacharya, Dong, and Yu, elsewhere in this book) is interesting because this procedure avoids the intrinsic randomness introduced by chemical substitution. Thus, it could potentially be expected that new phase diagrams may emerge employing oxide superlattices for the electronic doping procedure, as opposed to chemical doping via ionic substitution, which could be different from those of the alloy counterparts. This is certainly an exciting area of research worth pursuing.

In addition to quenched disorder *strain* is also an important factor to be considered in the study of transition metal oxides. For instance, by growing thin films of $\text{La}_{1-x}\text{Sr}_x\text{MnO}_3$ on different substrates, the lattice constants of LSMO can be modified, since they tend to adjust to the values corresponding to the substrate during the growing process. By this procedure the ratio c/a , where $c(a)$ is the lattice constant along the z axis (the x or y axes), can be

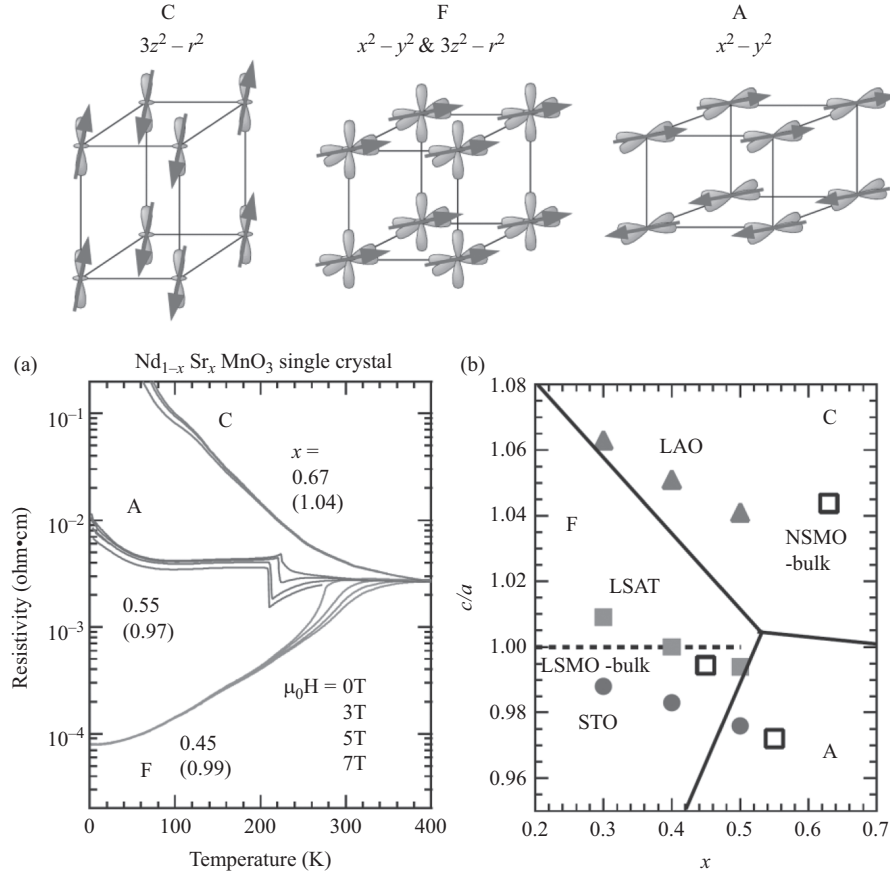


Fig. 1.19 A phase diagram of perovskite manganese oxides, reproduced from [1]. The top panel shows schematically the orbital and spin order realized in the hole-doped manganese oxides corresponding to C, F, and A-type phases. Lower panel (a) contains the temperature dependence of the resistivity in various magnetic fields for the case of $\text{Nd}_{1-x} \text{Sr}_x \text{MnO}_3$, and for the three phases at the top of the figure. The numbers in parentheses represent the uniaxial lattice strain, more specifically the c/a ratio, indicating the coupling of the magnetism to the orbital order. Lower panel (b) is the schematic phase diagram varying the lattice strain c/a and the doping level x . The data labelled LAO, LSAT, and STO represent results for the coherently strained epitaxial thin films of $\text{La}_{1-x} \text{Sr}_x \text{MnO}_3$ grown on the perovskite single-crystal substrates of LaAlO_3 , $(\text{La}, \text{Sr})(\text{Al}, \text{Ta})\text{O}_3$, and SrTiO_3 , respectively. LSMO-bulk and NSMO-bulk stand for the results for the bulk single crystals of $\text{La}_{1-x} \text{Sr}_x \text{MnO}_3$ and $\text{Nd}_{1-x} \text{Sr}_x \text{MnO}_3$, respectively. For details and references see [1].

altered and the relative stability of the competing FM, A-type AF, C-type AF, and G-type AF phases can be modified [41]. *Ab-initio* theoretical calculations [42] are in agreement with the experimental results. The importance of strain has also been remarked on in several other more recent theoretical [43, 44] and experimental [45, 46, 47] studies, and it provides an additional degree of freedom to control the properties of SCE materials. In fact, the phase diagrams of these compounds, which are routinely provided only in terms of the temperature and electronic concentration, should also include other axes, such as the strength of quenched disorder previously discussed, and the degree of strain, to fully understand the physics of these materials, as in Figure 1.19.

1.10 Outlook for correlated-electron technology: spintronics, double perovskites, multiferroics, orbitronics, resistance switching

The use of both the spin and charge degrees of freedom is an essential feature for the emerging field of spin-electronics, or spintronics [48]. Its straightforward application is control of the electrical current by an external magnetic field. In fact, invention of both the giant-magnetoresistive magnetic multilayer (composed of transition metals) and tunneling magnetoresistance (TMR) devices were crucial milestones for the field of spintronics and its industrial applications.

For general spintronic use, a half-metal, meaning a metallic ferromagnet with perfect spin polarization in the ground state, is of considerable importance. Several of the ferromagnetic metallic transition-metal oxides with strong electron correlation are expected to show such a half-metallic ground state, because of the potentially strong spin-charge coupling. The hole-doped manganites with a perovskite structure, such as $\text{La}_{1-x}\text{Sr}_x\text{MnO}_3$ ($0.2 < x < 0.5$), provide a typical example of a half-metal mediated by the previously discussed strong Hund coupling between the e_g itinerant electron spin and the t_{2g} localized spins. However, the TMR characteristics for the junction that uses $\text{La}_{1-x}\text{Sr}_x\text{MnO}_3$ are known to show unexpected degradation with increasing temperature, say, up to 200 K, despite the fact that their Curie temperatures are much higher (330–370 K). This seemingly rapid fading out of the spin polarization is believed to be due to modification of the interface magnetism of $\text{La}_{1-x}\text{Sr}_x\text{MnO}_3$ ($0.2 < x < 0.5$) when facing the insulating barrier. To attack this problem, alternative engineered magnetic interfaces are being explored extensively [49], as discussed in the remainder of the book. Moreover, the emerging novel properties and possible functionalities at the interfaces between correlated oxides [49, 50, 51] represent a new and important area for investigations, thus it is of considerable importance to study this issue. In the remainder of this book, several chapters will address this type of research at interfaces.

More robust and higher- T_C half-metals have also been sought for the family of perovskites to improve their performance in spintronic devices. A consequence of such investigations was discovery of the ordered double perovskite family with half-metallic characteristics, represented by $\text{Sr}_2\text{B}_1\text{B}_2\text{O}_6$ ($\text{B}_1 = \text{Fe}$ or Cr , $\text{B}_2 = \text{Mo}$ or Re) [52, 53]. In this class of compounds, the perovskite B (transition metal) sites are alternately occupied by two elements B_1 and B_2 in a rock-salt form. The valence of Fe (or Cr) is 3+, corresponding to the maximum spin state $S = 5/2(3/2)$. The Mo^{5+} ($4d^1$) or Re^{5+} ($5d^2$) ion provides the conduction electrons, partially hybridizing with

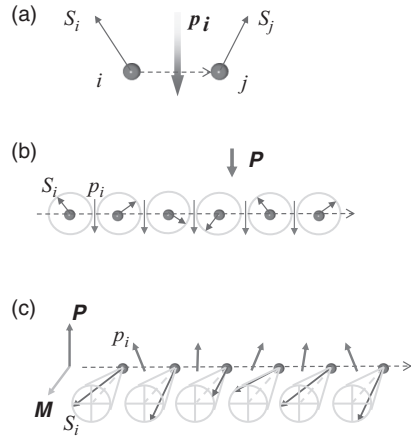


Fig. 1.20 Possible spin superstructures in multiferroics that can present a strong coupling between magnetism and electricity. (a) Canted spins on neighboring atomic sites. (b) Spin spiral structure producing a uniform polarization (P). (c) Conical spin structure allowing both uniform magnetization (M) and P .

the spin-down state of Fe or Cr, and strongly coupling antiferromagnetically with the local spins (spin-up states) on Fe or Cr. Thus, the states near the Fermi level are composed only of the spin-down electrons, forming the half-metallic ground state. The ferromagnetic transition temperature can be very high, for example, 420 K for $\text{Sr}_2\text{FeMoO}_6$ [52], and as high as 615 K for $\text{Sr}_2\text{CrReO}_6$ [53]. Possible antiferromagnetic metals with a half-metallic ground state, which is a highly spin-polarized state without any magnetization, have also been sought in the family of ordered perovskites [54, 55], but so far attempts have not been successful because of the correlation-induced charge-gap opening.

Another important group of compounds related to spintronic oxides are the multiferroics, materials with coexisting ferroelectric and magnetic orders, which can potentially host a gigantic magnetoelectric (ME) effect. Concerning the coupling between magnetism and ferroelectricity, a new simple scheme has recently been theoretically [56, 57, 58] and experimentally [59] demonstrated: mutually canted spins (such as in Figure 1.20(a)), that may be generated by spin frustration effects [60], can produce an electronic polarization through the spin-orbit interaction. When the spins form a transverse-spiral (cycloidal) modulation along a specific crystallographic direction (Figure 1.20(b)), then every nearest-neighbor pair produces a unidirectional polarization, p_i , which is proportional to the cross product between those nearest-neighbor spins, and, hence, a macroscopic polarization P should be generated. The direction of polarization may be fully determined by the clockwise or counterclockwise rotation of the spins that are proceeding along the spiral propagation axis, called the spin helicity.

In these cycloidal spin compounds, typically, perovskite TbMnO_3 and DyMnO_3 , spontaneous polarization can easily be controlled using an external magnetic field of a specific direction (since the magnetic field can control the orientation of the spin helicity), inducing generation and/or flipping of the spontaneous polarization [59], which can be viewed as a gigantic ME effect. Multiferroics based on this mechanism have also been realized in the conical

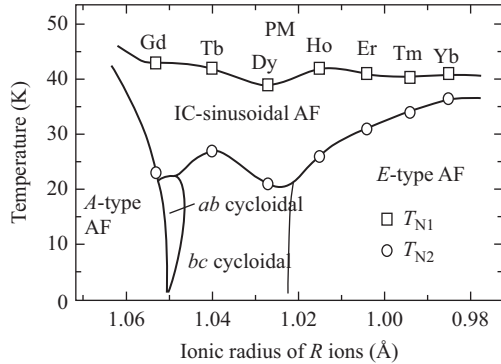


Fig. 1.21 Experimental phase diagram of the multiferroic manganites showing the A-type antiferromagnetic phase (that appears e.g. in LaMnO_3) followed, by reducing the rare earth radius R , by spin spiral (sinusoidal and cycloidal) phases, where ferroelectricity was found at low temperatures for the cycloidal arrangement, and finally ending with the E-type phase (which is a complex form of an antiferromagnetic state, involving zigzag chains) as the R radius is reduced further. More details can be found in [59] (see also [60] for a theoretical discussion and references).

spin state (Figure 1.20 (c)) where the transverse spiral component coexists with the uniform (spontaneous or field-induced) magnetization component along the cone axis, and hence, flexible control of the polarization vector is possible using external magnetic fields. These cycloidal and transverse-conical spin states are often observed in complex transition-metal compounds such as spinels and perovskites, where competing exchange interactions of neighboring spins can cause such a periodically modulated spin structure. As a natural extension of these studies, electrical control of the magnetization vector is currently being explored by several groups as a new and potentially important spintronic function.

To complete the discussion about multiferroics and in order to properly visualize these materials in the context of phase competition, Figure 1.21 shows the phase diagram of the undoped manganite multiferroics with generic chemical formula REMnO_3 [59]. Starting with decreasing the ionic radius of the rare earth element from La down to Gd, it is known that the ground state presents A-type antiferromagnetic characteristics. However, as chemical substitution of La by other RE elements proceeds further, the critical temperature toward the A-type AF phase clearly decreases and eventually a state with non-collinear spin order, and concomitant ferroelectric properties in view of the previous discussion, is stabilized. Finally, for the cases of Ho to Yb, another exotic state with so-called E-type antiferromagnetic order is stabilized. Thus, the spiral state that is needed for multiferroicity emerges from the competition between the A- and E-type antiferromagnetic states [60].

Note that hole- or electron-doped manganites may also induce the ferroelectric state as argued for their charge-orbital ordered states theoretically [61] or experimentally [62, 63]. Furthermore, recent computational studies have suggested that for sufficiently low bandwidth, the hole doping of the manganites may lead to a complex exotic state made from stripes that could be multiferroic [64]. While this prediction still remains to be tested experimentally, here

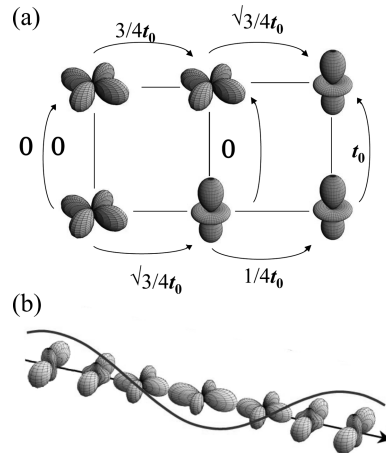


Fig. 1.22 (a) Electron hopping amplitudes between the nearest-neighbor sites involving the various orbital states shown. t_0 stands for the transfer integral unit. (b) Schematic representation of the quantal orbital wave, or orbiton, of the orbital-ordered state.

what it is important to remark is that the field of doped manganite multiferroics deserves considerable attention due to the potential for interesting surprises that still remains.

In analogy with spintronics, one can also consider the possibility of controlling electric currents through the d -electron orbital state [1]. This potential correlated-electron technology is called orbital-electronics or orbitronics [65]. In a broad context, the CMR phenomenon itself amounts to a field-induced modification of orbital correlation, and hence, it could provide one such example. By analogy to the magnetoresistance effect in the spin-ordered state, one can utilize the orbital degree of freedom to regulate the electrical conduction. For example, when the orbital ordering composed of $d_{x^2-y^2}$ orbitals is realized in the nearly cubic perovskite lattice, the charge dynamic is highly anisotropic, more specifically it is confined within the xy plane and insulating along the z direction, as can be seen from the transfer hopping values shown in Figure 1.22(a). In reality, such uniform orbital ordering is present ubiquitously in overdoped manganites, and a highly two-dimensional charge motion is observed despite the nearly cubic lattice structure [66].

The key idea of orbitronics is ultrafast switching of the orbital state, and hence of the related spin-charge state, by means of electric fields and/or light irradiation. Since the orbital shape, rod-like or planar, represents the electron's probability-density distribution, the orbital degree of freedom can inherently couple with the electric field through its anisotropic polarizability. In this context, the orbital manipulation might bear analogy to liquid-crystal technology, in which rod-shaped or planar molecules can respond to the electric field through their anisotropic polarizability.

To describe the dynamical response of the orbital to external fields, it is necessary to define the orbital wave or orbiton in the orbital-ordered state (Figure 1.22(b)). An advantage of the use of the orbital degree of freedom for the ultrafast control of electronic and magnetic states is that the orbiton frequency is high [67], 10–100 THz, as compared to the typical spin

32 A brief introduction to strongly correlated electronic materials

precession frequency (i.e. the $\mathbf{k} = \mathbf{0}$ magnon energy in a ferromagnet) of 1–100 GHz. In fact, in the initial process of photoinduced insulator–metal transition in the perovskite manganite ($\text{Pr}_{0.7}\text{Ca}_{0.3}\text{MnO}_3$), the orbiton mode of 30 THz is observed in ultrafast optical spectroscopy [68].

Correlated-electron science is thus exploiting a broad range of materials and electronic properties, in addition to the famous high- T_c and CMR-related phenomena that have received so much attention. Noteworthy is the recent advance of epitaxial-growth technology for transition-metal oxide thin films and superlattices, as well as discovery of many intriguing properties at the hetero-interfaces, described in more detail in several chapters of this book. At the interface, the spin and orbital, as well as charge, states are greatly modified, and they may be subject to external magnetic and/or electric fields that can induce large nonlinear effects. One of the potential applications of such phenomena is the *resistance switching* memory effect of the correlated-oxide interface with metal electrodes [69, 70]; the mechanisms are still to be clarified, but the possible application of this effect to high-density, fast, nonvolatile memory devices (resistive random-access memory, or ReRAM) is now being investigated extensively. Another interesting example is the creation of a polar ferromagnet with broken inversion symmetry at the interface [71, 72], in which many new intriguing magnetoelectronic functions, such as nonlinear/nonreciprocal magneto-optical and dynamical magnetoelectric effects, can be observed because of the simultaneous breaking of space-inversion and time-reversal symmetries.

1.11 Conclusions

The study of correlated electronic materials continues at a fast pace. Close interaction between theory and experiment has been crucial to progress in this field. The complexity of these compounds, manifested in their rich phase diagrams, self-organization, and nonlinear responses, suggests their potential use in devices. Even leaving aside technological applications, which will take considerable time to realize, the interesting properties of these materials clearly define an exciting field of fundamental scientific research that is full of surprises, and will surely continue to provide exciting and challenging phenomena in the near future.

Acknowledgments

E. Dagotto is supported by the U.S. Department of Energy, Office of Basic Energy Sciences, Materials Sciences and Engineering Division and by the National Science Foundation under Grant No. DMR-11-04386. The work of Y. Tokura was partly supported by the Funding Program for World-Leading Innovative R&D on Science and Technology (FIRST) on “Quantum Science on Strong-correlation”.

References

- [1] Tokura Y. and Nagaosa N. (2000). Orbital Physics in Transition-Metal Oxides. *Science* **288**, 462–468.
- [2] Dagotto E. (2005). Complexity in Strongly Correlated Electronic Systems. *Science* **309**, 257–262.
- [3] Mott N.F. (1990). *Metal-Insulator Transitions*. second edition. Taylor and Francis, London.

- [4] Dagotto E. and Tokura Y. (2008). Strongly Correlated Electronic Materials: Present and Future. *MRS Bulletin* **33**, 1037–1045.
- [5] Kamihara Y., Watanabe T., Hirano M., and Hosono H. (2008). Iron-Based Layered Superconductor $\text{La}[\text{O}_{1-x}\text{F}_x]\text{FeAs}$ ($x = 0.05\text{--}0.12$) with $T_c = 26$ K. *J. Am. Chem. Soc.* **130**, 3296–3297.
- [6] Lynn J.W. and Dai P. (2009). Neutron studies of the iron-based family of high T_c magnetic superconductors. *Physica C* **469**, 469–476; and references therein; Lumsden M.D. and Christianson A.D. (2010). Magnetism in Fe-based superconductors. *J. Phys.: Condens. Matter* **22**, 203203; and references therein; Johnston D.C. (2010). The puzzle of high temperature superconductivity in layered iron pnictides and chalcogenides. *Adv. Phys.* **59**, 803–1061 and references therein.
- [7] Yu R., Trinh K.T., Moreo A., et al. (2009). Magnetic and metallic state at intermediate Hubbard U coupling in multiorbital models for undoped iron pnictides. *Phys. Rev. B* **79**, 104510 (16 pages).
- [8] Committee on CMMP 2010. (2007). *Condensed-Matter and Materials Physics: The Science of the World Around Us*. National Academies Press, Washington, DC.
- [9] Basic Energy Sciences Advisory Committee (BESAC) Grand Challenges Subcommittee. (2007). *Directing Matter and Energy: Five Challenges for Science and the Imagination*. U. S. Department of Energy, Washington, DC.
- [10] Imada M., Fujimori A., and Tokura Y. (1998). Metal-insulator transitions. *Rev. Mod. Phys.* **70**, 1039–1263.
- [11] Torrance J.B., Lacorre P., Nazzal A.I., Ansaldo E.J., and Niedermayer Ch. (1992). Systematic study of insulator-metal transitions in perovskites RNiO_3 ($\text{R}=\text{Pr}, \text{Nd}, \text{Sm}, \text{Eu}$) due to closing of charge-transfer gap. *Phys. Rev. B* **45**, 8209–8212.
- [12] Dagotto E. (1994). Correlated electrons in high-temperature superconductors. *Rev. Mod. Phys.* **66**, 763–840; and references therein.
- [13] Armitage N.P., Fournier P., and Greene R.L. (2010). Progress and perspectives on electron-doped cuprates. *Rev. Mod. Phys.* **82**, 2421–2487; and references therein.
- [14] Tokura Y., Taguchi Y., Fujishima Y., et al. (1993). Filling dependence of electronic properties on the verge of metal–Mott–insulator transition in $\text{Sr}_{1-x}\text{La}_x\text{TiO}_3$. *Phys. Rev. Lett.* **70**, 2126–2129.
- [15] Okimoto Y., Katsufuji T., Okada Y., Arima T., and Tokura Y. (1995). Optical spectra in $(\text{La}, \text{Y})\text{TiO}_3$: Variation of Mott–Hubbard gap features with change of electron correlation and band filling. *Phys. Rev. B* **51**, 9581–9588; and references therein. See also [14].
- [16] Nakatsuji S., private communication. See also Nakatsuji S. and Maeno Y. (2000). Quasi-Two-Dimensional Mott Transition System $\text{Ca}_{2-x}\text{Sr}_x\text{RuO}_4$. *Phys. Rev. Lett.* **84**, 2666–2669; Nakatsuji S., Dobrosavljević V., Tanasković D., et al. (2004). Mechanism of Hopping Transport in Disordered Mott Insulators. *Phys. Rev. Lett.* **93**, 146401 (4 pages).
- [17] Tokura Y. (2006). Critical features of colossal magnetoresistive manganites. *Rep. Prog. Phys.* **69**, 797–852.
- [18] Foo M.L., Wang Y., Watauchi S., et al. (2004). Charge Ordering, Commensurability, and Metallicity in the Phase Diagram of the Layered Na_xCoO_2 . *Phys. Rev. Lett.* **92**, 247001 (4 pages).
- [19] Sawada H., Hamada N., Terakura K., and Asada K.T. (1996). Orbital and spin orderings in YVO_3 and LaVO_3 in the generalized gradient approximation. *Phys. Rev. B* **53**, 12742–12749.

34 A brief introduction to strongly correlated electronic materials

- [20] Kanamori J. (1959). Superexchange interaction and symmetry properties of electron orbitals. *J. Phys. Chem. Solids* **10**, 87–98.
- [21] Moreira dos Santos A., Cheetham A.K., Atou T., *et al.* (2002). Orbital ordering as the determinant for ferromagnetism in biferroic BiMnO_3 . *Phys. Rev. B* **66**, 064425 (4 pages).
- [22] Chen C.H., Cheong S.-W., and Cooper A.S. (1993). Charge modulations in $\text{La}_{2-x}\text{Sr}_x\text{NiO}_{4+y}$: Ordering of polarons. *Phys. Rev. Lett.* **71**, 2461–2464.
- [23] Tranquada J.M., Sternlieb B.J., Axe J.D., Nakamura Y., and Uchida S. (1995). Evidence for stripe correlations of spins and holes in copper oxide superconductors. *Nature* **375**, 561–563.
- [24] Kivelson S.A., Fradkin E., and Emery V.J. (1998). Electronic liquid-crystal phases of a doped Mott insulator. *Nature* **393**, 550–553.
- [25] Murakami Y., Kawada H., Kawata H., *et al.* (1998). Direct Observation of Charge and Orbital Ordering in $\text{La}_{0.5}\text{Sr}_{1.5}\text{MnO}_4$. *Phys. Rev. Lett.* **80**, 1932–1935.
- [26] Dagotto E., Hotta T., and Moreo A. (2001). Colossal Magnetoresistant Materials: The Key Role of Phase Separation. *Phys. Rep.* **344**, 1–153.
- [27] Yunoki S., Hu J., Malvezzi A., *et al.* (1998). Phase Separation in Electronic Models for Manganites. *Phys. Rev. Lett.* **80**, 845–848. For experimental studies also addressing phase separation see Uehara M., Mori S., Chen C.H., and Cheong S.-W. (1999). Percolative phase separation underlies colossal magnetoresistance in mixed-valent manganites. *Nature* **399**, 560–563.
- [28] Dagotto E. (2002). *Nanoscale Phase Separation and Colossal Magnetoresistance*. Springer-Verlag, Berlin.
- [29] Gomes K., Pasupathy A.N., Pushp A., *et al.* (2007). Visualizing pair formation on the atomic scale in the high-T_c superconductor $\text{Bi}_2\text{Sr}_2\text{CaCu}_2\text{O}_{8+\delta}$. *Nature* **447**, 569–572. For other STM results related with inhomogeneous states see for instance Lang K., Madhavan V., Hoffman J.E., *et al.* (2002). Imaging the granular structure of high-T_c superconductivity in underdoped $\text{Bi}_2\text{Sr}_2\text{CaCu}_2\text{O}_{8+\delta}$. *Nature* **415**, 412–416.
- [30] Alvarez G., Mayr M., Moreo A., and Dagotto E. (2005). Areas of superconductivity and giant proximity effects in underdoped cuprates. *Phys. Rev. B* **71**, 014514 (7 pages); Mayr M., Alvarez G., Moreo A., and Dagotto E. (2006). One-particle spectral function and local density of states in a phenomenological mixed-phase model for high-temperature superconductors. *Phys. Rev. B* **73**, 014509 (15 pages).
- [31] Alvarez G. and Dagotto E. (2008). Fermi Arcs in the Superconducting Clustered State for Underdoped Cuprate Superconductors. *Phys. Rev. Lett.* **101**, 177001 (4 pages).
- [32] Jin S., Tiefel T.H., McCormack M., *et al.* (1994). Thousandfold Change in Resistivity in Magnetoresistive La-Ca-Mn-O Films. *Science* **264**, 413–415.
- [33] Schiffer P., Ramirez A.P., Bao W., and Cheong S.-W. (1995). Low Temperature Magnetoresistance and the Magnetic Phase Diagram of $\text{La}_{1-x}\text{Ca}_x\text{MnO}_3$. *Phys. Rev. Lett.* **75**, 3336–3339.
- [34] Sen C., Alvarez G., and Dagotto E. (2010). First Order Colossal Magnetoresistance Transitions in the Two-Orbital Model for Manganites. *Phys. Rev. Lett.* **105**, 097203 (4 pages).
- [35] Sen C., Alvarez G., and Dagotto E. (2007). Competing Ferromagnetic and Charge-Ordered States in Models for Manganites: The Origin of the Colossal Magnetoresistance Effect. *Phys. Rev. Lett.* **98**, 127202 (4 pages); and references therein.

- [36] Burg J., Mayr M., Martin-Mayor V., Moreo A., and Dagotto E. (2001). Colossal Effects in Transition Metal Oxides Caused by Intrinsic Inhomogeneities. *Phys. Rev. Lett.* **87**, 277202 (4 pages).
- [37] For other techniques to handle this problem without diagonalizing exactly the fermionic sector at each step, see Kumar S. and Majumdar P. (2006). Insulator–Metal Phase Diagram of the Optimally Doped Manganites from the Disordered Holstein–Double Exchange Model. *Phys. Rev. Lett.* **96**, 016602 (4 pages); and references therein,
- [38] Tomioka Y. and Tokura Y. (2004). Global phase diagram of perovskite manganites in the plane of quenched disorder versus one-electron bandwidth. *Phys. Rev. B* **70**, 014432 (5 pages); and references therein.
- [39] Akahoshi D., Uchida M., Tomioka Y., et al. (2003). Random Potential Effect near the Bicritical Region in Perovskite Manganites as Revealed by Comparison with the Ordered Perovskite Analogs. *Phys. Rev. Lett.* **90**, 177203 (4 pages).
- [40] Rullier-Albenque F., Alloul H., Balakirev F., and Proust C. (2008). Disorder, metal–insulator crossover and phase diagram in high-T_c cuprates. *EPL* **81**, 37008 (6 pages); and references therein.
- [41] Konishi Y., Fang Z., Izumi M., et al. (1999). Orbital-State-Mediated Phase-Control of Manganites. *J. Phys. Soc. Jpn.* **68**, 3790–3793.
- [42] Fang, Z., Solovyev I.V., and Terakura K. (2000). Phase Diagram of Tetragonal Manganites. *Phys. Rev. Lett.* **84**, 3169–3172.
- [43] Ahn K.H., Lookman T., and Bishop A.R. (2004). Strain-induced metal–insulator phase coexistence in perovskite manganites. *Nature* **428**, 401–404.
- [44] Dong S., Yunoki S., Zhang X., et al. (2010). Highly anisotropic resistivities in the double-exchange model for strained manganites. *Phys. Rev. B* **82**, 035118 (6 pages).
- [45] Wu W., Israel C., Hur N., et al. (2006). Magnetic imaging of a supercooling glass transition in a weakly disordered ferromagnet. *Nature Mater.* **5**, 881–886; Yamada H., Kawasaki M., Lottermoser T., Arima T., and Tokura Y. (2006). LaMnO₃/SrMnO₃ interfaces with coupled charge-spin-orbital modulation. *Appl. Phys. Lett.* **89**, 052506 (3 pages); Dhakal T., Tosado J., and Biswas A. (2007). Effect of strain and electric field on the electronic soft matter in manganite thin films. *Phys. Rev. B* **75**, 092404 (4 pages); Dekker M.C., Rata A.D., Boldyreva K., et al. (2009). Colossal elastoresistance and strain-dependent magnetization of phase-separated (Pr_{1-y}La_y)_{0.7}Ca_{0.3}MnO₃ thin films. *Phys. Rev. B* **80**, 144402 (7 pages); Ding Y., Haskel D., Tseng Y.-C., et al. (2009). Pressure-Induced Magnetic Transition in Manganite (La_{0.75}Ca_{0.25}MnO₃). *Phys. Rev. Lett.* **102**, 237201 (4 pages).
- [46] Ward T.Z., Budai J.D., Gai Z., et al. (2009). Elastically driven anisotropic percolation in electronic phase-separated manganites. *Nature Phys.* **5**, 885–888; and references therein.
- [47] Yamada H., Ogawa Y., Ishii Y., et al. (2004). Engineered Interface of Magnetic Oxides. *Science* **305**, 646–648.
- [48] Zutic I., Fabian J., and Das Sarma S. (2004). Spintronics: Fundamentals and applications. *Rev. Mod. Phys.* **76**, 323–410; and references therein.
- [49] Ohtomo A. and Hwang H.Y. (2004). A high-mobility electron gas at the LaAlO₃/SrTiO₃ heterointerface. *Nature* **427**, 423–426.
- [50] Reyren N., Thiel S., Caviglia A.D., et al. (2007). Superconducting Interfaces Between Insulating Oxides. *Science* **317**, 1196–1199. For additional references see also Dagotto E. (2007). When Oxides Meet Face to Face. *Science* **318**, 1076–1077.

36 A brief introduction to strongly correlated electronic materials

- [51] Okamoto S., and Millis A. (2004). Electronic reconstruction at an interface between a Mott insulator and a band insulator. *Nature* **428**, 630–633.
- [52] Kobayashi K.I., Kimura T., Sawada H., Terakura K., and Tokura Y. (1998). Room-temperature magnetoresistance in an oxide material with an ordered double-perovskite structure. *Nature* **395**, 677–680.
- [53] Kato H., Okuda T., Okimoto Y., Tomioka Y., Takenoya Y., Ohkubo A., Kawasaki M., and Tokura Y. (2002). Metallic ordered double-perovskite $\text{Sr}_2\text{CrReO}_6$ with maximal Curie temperature of 635 K. *Appl. Phys. Lett.* **81**, 328 (3 pages).
- [54] Pickett W.E. (1996). Single Spin Superconductivity. *Phys. Rev. Lett.* **77**, 3185–3188.
- [55] Pardo V. and Pickett W.E. (2009). Compensated magnetism by design in double perovskite oxides. *Phys. Rev. B* **80**, 054415 (6 pages).
- [56] Katsura H., Nagaosa N., and Balatsky A.V. (2005). Spin Current and Magnetoelectric Effect in Noncollinear Magnets. *Phys. Rev. Lett.* **95**, 057205 (4 pages).
- [57] Sergienko I.A., and Dagotto E. (2006). Role of the Dzyaloshinskii-Moriya interaction in multiferroic perovskites. *Phys. Rev. B* **73**, 094434 (5 pages).
- [58] Sergienko I.A., Sen C., and Dagotto E. (2006). Ferroelectricity in the Magnetic E-Phase of Orthorhombic Perovskites. *Phys. Rev. Lett.* **97**, 227204 (4 pages); Picozzi S., Yamauchi K., Sanyal B., Sergienko I. A., and Dagotto E. (2007). Dual Nature of Improper Ferroelectricity in a Magnetoelectric Multiferroic. *Phys. Rev. Lett.* **99**, 227201 (4 pages).
- [59] Ishiwata S., Kaneko Y., Tokunaga Y., Taguchi Y., et al. (2010). Perovskite manganites hosting versatile multiferroic phases with symmetric and antisymmetric exchange strictions. *Phys. Rev. B* **81**, 100411(R) (4 pages); and references therein. See also Kimura T., Goto T., Sintani H., et al. (2003). Magnetic control of ferroelectric polarization. *Nature* **426**, 55–58.
- [60] Dong S., Yu R., Yunoki S., Liu J.-M., and Dagotto E. (2008). Origin of multiferroic spiral spin order in the RMnO_3 perovskites. *Phys. Rev. B* **78**, 155121 (6 pages); and references therein.
- [61] Efremov D.V., van den Brink J., and Khomskii D. (2005). Bond centered versus site-centered charge ordering: ferroelectricity in oxides. *Physica B* **359**, 1433–1435.
- [62] Tokunaga Y., Lotteroser Th., Lee Y.S., et al. (2006). Rotation of orbital stripes and the consequent charge-polarized state in bilayer manganites. *Nature Mat.* **5**, 937–941.
- [63] Lopes A.M.L., Araujo J.P., Amaral V.S., et al. (2008). New Phase Transition in the $\text{Pr}_{1-x}\text{Ca}_x\text{MnO}_3$ System: Evidence for Electrical Polarization in Charge Ordered Manganites. *Phys. Rev. Lett.* **100**, 155702 (4 pages).
- [64] Dong S., Yu R., Liu J.-M., and Dagotto E. (2009). Striped Multiferroic Phase in Double-Exchange Model for Quarter-Doped Manganites. *Phys. Rev. Lett.* **103**, 107204 (4 pages); and references therein.
- [65] Tokura Y. (2003). Correlated-Electron Physics in Transition-Metal Oxides. *Physics Today* **56**, 50–55.
- [66] Kuwahara H., Okuda T., Tomioka Y., Asamitsu A., and Tokura Y. (1999). Two-Dimensional Charge-Transport and Spin-Valve Effect in the Layered Antiferromagnet $\text{Nd}_{0.45}\text{Sr}_{0.55}\text{MnO}_3$. *Phys. Rev. Lett.* **82**, 4316–4319.
- [67] Saitoh E., Okamoto S., Takahashi K.T., et al. (2001). Observation of orbital waves as elementary excitations in a solid. *Nature* **410**, 180–183.
- [68] Polli D., Rini M., Wall S., et al. (2007). Coherent orbital waves in the photo-induced insulator–metal dynamics of a magnetoresistive manganite. *Nature Mat.* **6**, 643–647.

- [69] Lu S.Q., Wu N.J., and Ignatiev A. (2000). Electric-pulse-induced reversible resistance change effect in magnetoresistive films. *Appl. Phys. Lett.* **76**, 2749 (3 pages).
- [70] Sawa A., Fujii T., Kawasaki M., and Tokura Y. (2004). Hysteretic current-voltage characteristics and resistance switching at a rectifying Ti/Pr_{0.7}Ca_{0.3}MnO₃ interface. *Appl. Phys. Lett.* **85**, 4073 (3 pages).
- [71] Yamada H., Ogawa Y., Kawasaki M., and Tokura Y. (2002). Perovskite oxide tricolor superlattices with artificially broken inversion symmetry by interface effects. *Appl. Phys. Lett.* **81**, 4793 (3 pages).
- [72] Kida N., Yamada H., Sato H., *et al.* (2007). Optical Magnetoelectric Effect of Patterned Oxide Superlattices with Ferromagnetic Interfaces. *Phys. Rev. Lett.* **99**, 197404 (4 pages).